Temporal evolution of shallow marine diagenetic environments: Insights from carbonate concretions

Sean J. Loyd[a,*], Patrick Meister[b], Bo Liu[c], Kevin Nichols[d], Frank A. Corsetti[e], Robert Raiswell[f], William Berelson[e], Graham Shields[g], Mark Hounslow[h,i], John W.F. Waldron[j], Bayne Westrick-Snapp[a], Jamie Hoffman[a]

[a]Department of Geological Sciences, California State University, Fullerton, Fullerton CA 92831, United States
[b]Department of Geology, University of Vienna, Vienna, Austria
[c]Alfred-Wegener Institute Helmholtz Center for Polar and Marine Research, Bremerhaven, Germany
[d]Department of Mathematics, California State University, Fullerton, Fullerton CA 92831, United States
[e]Department of Earth Sciences, University of Southern California, Los Angeles CA 90089, United States
[f]School of Earth and Environment, University of Leeds, Leeds LS2 9JT, United Kingdom
[g]Department of Earth Sciences, University College London, London, WC1E 6BT, United Kingdom
[h]CEMP, Geography Department, Lancaster Environment Centre, Lancaster University, Lancaster, LA1 4YW, United Kingdom
[i]Department of Earth, Ocean and Ecological Sciences, University of Liverpool, Liverpool, L69 3GP, United Kingdom
[j]Department of Earth and Atmospheric Sciences, University of Alberta, Edmonton AB T6G 2E3, Canada

*Corresponding author (sloyd@fullerton.edu)

Abstract

Early diagenesis of marine organic matter dramatically impacts Earth's surface chemistry by changing the burial potential of carbon and promoting the formation of authigenic mineral phases including carbonate concretions. Marine sediment-hosted carbonate concretions tend to form as a result of microbial anaerobic diagenetic reactions that degrade organic matter and methane, some of which require an external oxidant. Thus, temporal changes in the oxidation state of Earth's oceans may impart a first-order control on concretion authigenesis mechanisms through time. Statistically significant variability in concretion carbonate carbon isotope compositions indicates changes in shallow marine sediment diagenesis associated with Earth's evolving redox landscape. This variability manifests itself as an expansion in carbon isotope composition range broadly characterized by an increase in maximum and decrease in minimum isotope values through time. Reaction transport modelling helps to constrain the potential impacts of shifting redox chemistry and highlights the importance of organic carbon delivery to the seafloor, marine sulfate concentrations, methane production and external methane influx. The first appearance of conclusively anaerobic oxidation of methane-derived concretions occurs in the Carboniferous and coincides with a Paleozoic rise in marine sulfate. The muted variability recognized in older concretions (and in particular for Precambrian concretions) likely reflects impacts of a smaller marine sulfate reservoir and perhaps elevated marine dissolved inorganic carbon concentrations. Causes of the increase in carbon isotope maximum values through time are more confounding, but may be related to isotopic equilibration of dissolved inorganic carbon with externally derived methane. Ultimately the concretion isotope record in part reflects changes in organic

matter availability and marine oxidation state, highlighting connections with the subsurface biosphere and diagenesis throughout geologic time.

1. INTRODUCTION

Carbonate concretions are isolated zones of relatively high cement content in sediments and sedimentary rocks (Coleman, 1993). These precipitates can exhibit textural and compositional characteristics that indicate initial formation within shallow sediments. Shallow formation indicators include deflection of external lamination (Raiswell, 1971), preservation of delicate primary sedimentary features (such as thin walled shells and macrofauna carcasses) (Allison and Pye, 1994; Blome and Albert, 1985; Bramlette, 1946; El Albani et al., 2001; Heimhofer et al., 2017; Martill, 1988), evidence of biological interaction by burrowing organisms (Bjørlykke, 1973; Hesselbo and Palmer, 1992; Savrda and Bottjer, 1988), erosional exhumation (Hesselbo and Palmer, 1992) and low proxy-based formation temperatures (Dale et al., 2014; Loyd et al., 2012). Therefore, carbonate concretions can result (at least initially) from relatively shallow diagenetic processes that are intimately related to the chemical composition of marine bottom waters and the availability of organic matter delivered to the sediment-water interface. The geochemistry of Earth's marine environments has experienced significant temporal variability in part associated with an overall increase in oxidation state (Lyons et al., 2014), associated fluctuations in marine chemistry (Canfield, 1998) and changes in organic carbon export (Krause et al., 2022; Krissansen‐Totton et al., 2021; Planavsky et al., 2022) and organic matter composition (Brocks et al., 2017). In particular, variable

92 organic carbon delivery to the seafloor and marine oxidant abundances (see below) likely
93 impacted shallow diagenetic processes related to remineralization.
94 Marine sediment-hosted carbonate concretions seem to form in association with
95 reactions that involve the microbial degradation of particulate organic matter and/or
96 methane (Irwin et al., 1977). Of these reactions, those considered most important for
97 concretion formation are iron reduction, organotrophic sulfate reduction, methanogenesis
98 and the anaerobic oxidation of methane (AOM) (Claypool and Kaplan, 1974; Coleman,
99 1993; Irwin et al., 1977; Orphan et al., 2004). The carbon isotope composition of
100 porewater DIC ($\delta^{13}C_{DIC}$) is impacted by the relative contributions of these pathways
101 wherein organic matter and methane oxidation reactions cause porewater $^{13}C_{DIC}$ depletion
102 and methanogenesis causes porewater $^{13}C_{DIC}$ enrichment. The magnitude of isotope
103 enrichments and depletions is dictated by oxidant supply and reduced carbon source
104 (organic matter or methane), among other factors (e.g., Meister et al., 2019). Carbonate
105 concretions inherit the carbon isotope composition of porewater DIC owing to minimal
106 isotope fractionation during carbonate precipitation (Emrich et al., 1970; Ohmoto and
107 Rye, 1979). Thus, concretion carbon isotope compositions and can be used to track
108 carbon-phase reactants (organic matter or methane) and/or reaction pathways of shallow
109 marine diagenetic environments through time.
110 Here, carbonate concretion abundance and carbon isotope data (consisting of both
111 new and previously reported data) are used to characterize ancient marine shallow
112 diagenetic environments. These data are assessed through a transient reaction transport
113 model to explore potential impacts of contemporaneous environmental changes.
114 Ultimately, we show that amplified variability in concretion carbon isotope signatures

115 coincides with proposed increases in organic carbon export and marine sulfate
116 concentrations, implicating these factors as important for diagenetic carbonate
117 mineralization throughout geologic time. Modeling results suggest that external methane
118 inputs are likely required to generate severe ^{13}C depletions in concretionary carbonate.
119 Elevated marine dissolved inorganic carbon (DIC) contents may also play a role by
120 muting porewater isotope variability during much of the Precambrian. In addition, we
121 identify potentially counterintuitive coincident changes in methanogenesis-driven
122 diagenesis during the Phanerozoic.
123

124 **2. METHODS**

125 Marine sediment-hosted carbonate concretion occurrence and carbonate carbon
126 isotope composition ($\delta^{13}C_{con}$) data (~5,000 data points from ~170 units) were primarily
127 compiled from published reports. New $\delta^{13}C_{con}$ data were collected from select time
128 periods where isotope data have not been reported (see Supplementary Tables 1, 2). Host
129 rock formation name, age, and lithology, and concretion mineralogy, crystallographic
130 habit (for septarian concretions), carbon and oxygen isotope data were also collected
131 (Supplementary Tables 1, 2 and 3), as available. Similar information provided for
132 authigenic carbonates recovered from siliciclastic marine sediments is provided for
133 comparison (Supplementary Table 4). Most new concretion data were generated from
134 powders of slabbed samples using a Dremel® rotary tool fitted with a 3-mm carbide drill
135 bit. Triplicate 5-7 mg splits of concretion powders were dissolved in 10% phosphoric
136 acid in sealed and evacuated exetainer vials. The carbon isotope composition of produced
137 CO_2 was determined using a G2121-i Picarro® Cavity Ringdown Spectrometer (CRDS)

138 via introduction through an Automate® carbonate preparation device. Limited additional
139 new carbon isotope data from the Chuar Group (nine data points) were generated using a
140 VG Instruments PRISM II isotope ratio mass spectrometer after sample dissolution in a
141 common acid bath at 90°C. Isotope compositions reported in the typical delta (δ) notation
142 in permil (‰) versus the VPDB standard. Isotope values were determined by comparison
143 with international [IAEA NBS-18 ($\delta^{13}C$ = –5.014‰, $\delta^{18}O$ = –23.2‰), Carrara Marble
144 ($\delta^{13}C$ = +2.46‰, $\delta^{18}O$ = –2.37‰), NIST SRM 915B ($\delta^{13}C$ = –8.53)] and laboratory
145 [CRCP90 ($\delta^{13}C$ = –4.13‰), CRC200 ($\delta^{13}C$ = +2.12‰), WD-1A ($\delta^{13}C$ = –42.61‰)]
146 standards. New carbon isotope data reproducibility was better than +/– 1.0‰ (2 s.d.).
147 Statistical parameter estimation of the mean, variance, minimum, maximum and
148 range of carbon isotope data was accomplished via bootstrapping (Efron, 1979) across
149 select time periods (Supplementary Table 5). Biases in estimating extrema were
150 simulated empirically from repeated resampling, and then applied to adjust distributions
151 for parameter estimation of maximum and minimum values (Efron, 1982). Confidence
152 intervals (95%) for each numerical summary across the selected time periods were
153 generated via the bootstrap empirical distributions, as were pairwise statistical hypothesis
154 tests between each pairwise combination of selected time periods.
155 The factors that control potential ranges in carbon isotope compositions were
156 evaluated using a previously described transient reaction transport model (Meister et al.,
157 2013; Meister et al., 2019). This model was developed in part to constrain transport and
158 biogeochemical impacts on isotope compositions of the dominant carbon-containing
159 porewater phases. Marine sulfate concentrations, organic carbon content at the sediment-
160 water interface, external methane delivery, isotope fractionation during methanogenesis

and marine DIC contents were varied to explore impacts on porewater DIC isotope compositions. Here, complete ranges in porewater $\delta^{13}C_{DIC}$ values (including maxima and minima) are explored without predicting specific depths of carbonate authigenesis (in contrast to Laakso and Schrag (2020)). The modelled porewater isotope compositions are thus reflective of all of the possible concretion isotope compositions, resolving potential uncertainties in mineralization depth (e.g., Meister et al., 2019). Model inputs and parameterizations are provided in the Supplementary Materials ("Modelling Approach"), as is a diagram demonstrating how maximum and minimum values were determined (Supplementary Figure 1). Model results are compared to the ancient concretion carbon isotope record to identify potential drivers of temporal variability, they are not intended to recreate specific intervals of the record.

3. RESULTS

Carbonate concretions have been identified in 379 geologic formations. Of these units, carbon isotope data have been compiled or generated from 173, representing ~ 46% $\delta^{13}C_{con}$ coverage. The age distribution of carbonate concretions is not uniform; the vast majority have been identified in units younger than 600 Ma (Figure 1). An exception to this broad temporal trend is a relatively short-lived, concretion-abundant interval between ~2150 to 1750 Ma (Figure 2b). Within the Phanerozoic, concretion occurrence generally increases (aside from a few exceptions) up to the modern (Figure 1c). As has been recognized in a previous compilation (Mozley and Burns, 1993) concretions mostly occur within shale hosts (Figure 2a) and calcite represents the dominant mineralogy (Figure 2b).

184 Carbon isotope compositions range from –54.0 to +32.5‰ for the entire data set.
185 Absolute $\delta^{13}C_{con}$ values provide only limited insight into concretion formation
186 mechanisms. These data must be corrected to account for the contemporaneous seawater
187 $\delta^{13}C$ value, which represents the starting condition that is subsequently modified
188 by shallow diagenetic processes. This correction is relatively unimportant for Cenozoic
189 concretions because seawater $\delta^{13}C$ does not significantly deviate from 0‰. However, a
190 growing body of primary carbonate (i.e., non-diagenetic) carbon isotope data suggests
191 that seawater $\delta^{13}C$ was significantly different in earlier time periods (in particular during
192 intervals within the Proterozoic), in some cases reaching values as high as +11
193 (e.g., Maheshwari et al., 2010) to as low as –12‰ (e.g., Halverson et al., 2005). In order
194 to account for changes in seawater carbon isotope compositions, the quantity $\Delta^{13}C_{con\text{-}sw}$ is
195 defined as $\Delta^{13}C_{con\text{-}sw} = \delta^{13}C_{con} - \delta^{13}C_{sw}$, where $\delta^{13}C_{sw}$ is the contemporaneous seawater
196 carbon isotope composition as determined by either 1) the primarily Phanerozoic curve of
197 Veizer et al. (1999) or 2) stratigraphically nearby non-diagenetic carbonate beds. The
198 $\Delta^{13}C_{con\text{-}sw}$ parameter presented in Figure 4 thus reflects specific diagenetic pathways more
199 directly than $\delta^{13}C_{con}$. Uncertainties related to the primary carbonate $\delta^{13}C$ value and
200 temporal variability in isotope fractionation associated with organic matter production
201 (e.g., isotopic differences between contemporaneous marine DIC and organic carbon
202 varying between ~30 and 25‰, Kump and Arthur, 1999) are accounted for by the gray
203 solid and dashed bands in Figure 3.
204 Values of $\Delta^{13}C_{con\text{-}sw}$ exhibit significant changes since ~2800 Ma (Figure 3), as
205 outlined below.
206

- Archean concretion samples from ~2800, 2603 and 2600 Ma units yield $\Delta^{13}C_{con\text{-}sw}$ values that range from +9.9 to +15.0‰, –4.5 to +1.8‰ and +0.9 to +2.4‰, respectively.
- Early Proterozoic concretions (of the ~2150 to 1750 Ma interval discussed above) show $\Delta^{13}C_{con\text{-}sw}$ values that range from –24.5 to +1.4‰. ~1400 Ma concretions express $\Delta^{13}C_{con\text{-}sw}$ from –1.1 to +1.9‰.
- Concretions from a single middle Neoproterozoic site (~745 Ma) exhibit $\Delta^{13}C_{con\text{-}sw}$ values ranging from –15.6 to –7.9‰.
- Late Neoproterozoic (~560 and 555 Ma) carbonate concretions exhibit $\Delta^{13}C_{con\text{-}sw}$ values from –3.5 to +5.4‰.
- Cambrian to Devonian (542-360 Ma) concretions display an increased range in $\Delta^{13}C_{con\text{-}sw}$, with values extending from ~ –25.3‰ to +24.5‰.
- Younger concretions within Carboniferous to Permian sedimentary rocks express $\Delta^{13}C_{con\text{-}sw}$ values extending from –54.6 to +9.5‰.
- Triassic to Holocene concretions yield $\Delta^{13}C_{con\text{-}sw}$ values ranging from –55.7 to +31.5‰.

For comparison, marine sedimentary authigenic carbonate data (compiled in Supplementary Table 4, after Loyd and Smirnoff (2022)) are also provided. Note that sedimentary authigenic carbonates characterized as “modern”, may rather have formed at any time since the ages of the host sediment (host sediment ages provided in Supplementary Table 4). Similarly, carbonate concretions must have formed after deposition of the host rock. However, given that these precipitates form relatively soon

after deposition, concretion ages are here approximated as the same as their host sediment. Means, minima, maxima and ranges are provided for the above age groupings in Figure 4; histograms are displayed in Supplementary Figure 2, and statistical similarity analyses are provided in Supplementary Table 5.

As with primary carbonate phases, concretions may be altered by later diagenetic processes that overprint original carbon isotope compositions as often indicated by ^{18}O-depleted compositions (Bojanowski et al., 2014; Gross and Tracey Jr, 1966; Seewald, 2003). To screen for potential late diagenetic impacts on the temporal record, plots limited to samples expressing oxygen isotope compositions > –10‰ and > –5‰ have been generated (Supplementary Figure 3). These plots express similar trends as the complete record, suggesting that later diagenetic alteration does not strongly influence the broad temporal trends in $\Delta^{13}C_{con\text{-}sw}$.

4. DISCUSSION

The concretion occurrence and carbon isotope data presented here provide a more detailed picture of a temporal variability hypothesized by previous researchers (Melezhik and Fallick, 1996). The potential controls of this distribution are discussed below. Firstly, the quantities of concretion-bearing units and preserved marine sedimentary formations are compared to determine if variability can be explained simply by changes in the amount of rock preserved. Then, the major shifts in concretion carbon isotope composition are assessed in the context of potential controls on early marine diagenesis and mineralization.

4.1. Insights from the concretion record

The ability to assess the evolution of Earth-surface environments is increasingly challenging as we move back in time due to the limited preservation of older rocks. In addition, ongoing research shows that the mass of preserved sedimentary rock is not readily explained by erosive processes alone. Instead, changes in the Earth-surface system have likely impacted the production of sedimentary rock through time (Husson and Peters, 2018; Ronov et al., 1980). Reconstructions of the temporal abundance of passive margins (Bradley, 2008) and the quantity and volume of marine sedimentary rock formations (preserved on the North American continent) correlate with the quantity of concretion-bearing units (Supplementary Figure 4). Therefore, an environmental signal cannot be confidently identified even though a clear temporal change in concretion-containing units is evident. The concretion abundance record may also be obscured by reporting biases in the literature, the dominant data source for this compilation. As a result, the remaining discussion focuses on concretion carbon isotope data ($\Delta^{13}C_{con\text{-}sw}$) and potential controls on its variability.

The carbon isotope composition of a carbonate concretion is inherited from the porewater DIC from which it precipitates. Since there is only minimal isotope fractionation associated with carbonate mineral production (Emrich et al., 1970; Ohmoto and Rye, 1979), carbonate concretions provide a unique proxy for ancient diagenetic settings. The carbon isotope composition of DIC in porewater reflects a mixture of carbon derived from seawater, the oxidation of organic matter and the oxidation of methane. In addition, methanogenesis exhibits a significant isotope fractionation (Whiticar, 1999) that can further impact porewater DIC. The ranges in isotope

276 composition expressed in marine sediment porewaters result from the relative importance
277 of these different reactions in addition to the transport of carbon-containing reactants and
278 products (Zeebe, 2007). Oxidation- and organic matter-dependent reactions appear to
279 typify much of Earth history, as evidenced by the widespread occurrence of negative
280 values of $\Delta^{13}C_{con\text{-}sw}$. These reactions require external reactant(s), potentially including
281 aqueous sulfate and particulate iron oxide, and organic matter and/or methane carbon
282 sources. A growing body of research provides insight into the relative temporal
283 abundances of some of these phases. The following discussion explores reactant
284 variability and then connects these trends to specific characteristics of the $\Delta^{13}C_{con\text{-}sw}$
285 record to evaluate the evolution of marine diagenetic environments.
286
287 **4.2. Organic matter as a carbon source for carbonate precipitation**
288 The dominant concretion-forming mechanisms in marine sediments involve the
289 anaerobic degradation of organic matter or methane (Claypool and Kaplan, 1974;
290 Coleman, 1993; Irwin et al., 1977). Methane primarily forms by the degradation of
291 organic matter, either directly through fermentation reactions or indirectly through the
292 reduction of carbon dioxide derived from organic matter (Koyama, 1963; McCarty,
293 1964). Therefore, all of the major reaction pathways that lead to concretion
294 precipitation involve organic matter in one way or another.
295 The amount of marine carbon buried as organic matter has changed through time
296 (Figure 5), partially in concert with shifts in the oxidation state of Earth's surface (Krause
297 et al., 2022; Krissansen‐Totton et al., 2021; Planavsky et al., 2022). Our ability to assess
298 carbon burial relies primarily on temporal changes in the carbon isotope compositions of

299 primary marine carbonates, which approximately record the isotope composition of
300 oceanic DIC at the time of deposition (Schidlowski et al., 1975). Assuming that marine
301 carbonate $\delta^{13}C$ changes reflect steady-state oceanic inorganic carbon budgets, increases
302 correspond to enhanced organic carbon burial whereas decreases reflect increased organic
303 carbon destruction (i.e., oxidation) (Kump and Arthur, 1999). Although the $\delta^{13}C$
304 composition of limestones and dolostones preserved in the geologic record may not
305 faithfully record original marine conditions (e.g., Knauth and Kennedy, 2009), long-lived
306 and global positive carbon isotope excursions are difficult to explain without invoking
307 primary marine drivers. In particular, the ~2.3 to 2.1 Ga Lomagundi excursion
308 corresponds to a large ~ +10‰ carbonate carbon isotope swing (e.g., Schidlowski et al.,
309 1976) thought to be related to massive deposition of organic matter and an increase in
310 atmospheric O_2 (e.g., Eguchi et al., 2020; Karhu and Holland, 1996). Although the
311 Lomagundi positive isotope excursion has been interpreted as a diagenetic signal related
312 to methane production (Hayes and Waldbauer, 2006), contemporaneous trends in sulfur
313 and sulfur isotope geochemistry are more parsimoniously interpreted as consistent with a
314 primary origin (Planavsky et al., 2012). The Lomagundi event overlaps with the
315 beginning of the concretion-abundant interval between ~2.15 to 1.75 Ga (Figure 1a, b)
316 (Melezhik and Fallick, 1996). In addition to enhanced organic matter burial,
317 contemporaneous changes in the redox state of the oceans at this time may have yielded
318 complementary conditions required to stimulate sedimentary diagenesis, such as the
319 introduction of other oxidants to Earth's surface environment (see section 4.3 below).
320 Similar, long-lived primary carbonate positive $\delta^{13}C$ values ($\geq$ +5‰) occur
321 between glacial intervals in the post-~800 Ma Cryogenian Period (Halverson et al.,

322 2005). These ^{13}C-enriched values are likewise interpreted to represent the enhanced
323 burial of organic matter (Derry et al., 1992; Des Marais et al., 1992) and recent modeling
324 results support these findings (Kipp et al., 2021; Krause et al., 2022; Krissansen‐Totton
325 et al., 2021; Planavsky et al., 2022). Beginning about the same time (~750 Ma) and
326 extending toward the Proterozoic–Cambrian boundary, a transition in clay mineral
327 production may have facilitated enhanced burial of organic matter (Kennedy et al., 2006;
328 Kennedy et al., 2002). However, the direct impacts of this transition on atmospheric
329 oxygen contents have been challenged (Tosca et al., 2010). In addition, labile organic
330 matter that is buried in clay-rich sediments can be protected from degradation (Keil et al.,
331 1994), complicating the ability to predict potential impacts of secular changes in clay
332 production on shallow diagenetic environments.
333 Temporal variability in the total organic carbon (TOC) contents of marine shales
334 also provides support for fluctuating organic carbon burial (Och and Shields-Zhou, 2012;
335 Sperling and Stockey, 2018). Importantly, TOC contents increase significantly across the
336 Neoproterozoic–Cambrian boundary and remain relatively high throughout the
337 Phanerozoic (Sperling and Stockey, 2018) as also supported by modeled reconstructions
338 of organic matter burial rates (Krause et al., 2022; Krissansen‐Totton et al., 2021;
339 Planavsky et al., 2022). Shallow-marine diagenesis may have been stimulated as a result
340 of this high organic carbon burial rate.
341 Recent work has also revealed a profound shift in the nature of marine organic
342 matter between the Cryogenian “Snowball Earth” glacial intervals (~659 to 645 Ma).
343 Biomarker data suggest a transition from a dominantly bacterial to a bacterial and
344 eukaryotic marine planktonic biosphere (Supplementary Figure 5) (Brocks et al., 2017).

345 This expansion in marine biosphere diversity may have heralded contemporaneous
346 changes in organic matter reactivity. Organic matter reactivity impacts the efficiency of
347 remineralization (e.g., Burdige, 2007) and can influence degradation pathway (Meister et
348 al., 2013). However, the relationship between organic matter source (eukaryotic versus
349 non-eukaryotic) and general reactivity remains poorly understood. Therefore, the addition
350 of significant eukaryotic biomass may or may not have increased the reactivity of organic
351 matter and thus stimulated shallow diagenesis. The record of carbonate concretions since
352 ~659 to 645 Ma exhibits its own interesting trends, perhaps related to two subsequent
353 biological transitions, the appearance and proliferation of metazoans and land plants
354 (Supplementary Figure 5).

355 Partially decayed carcasses of animals, including bones and calcium carbonate or
356 phosphate shells, sometimes occur within carbonate concretions (El Albani et al., 2001;
357 Gaines et al., 2005; Yoshida et al., 2015). Such materials may have provided triggers for
358 localized remineralization and carbonate precipitation since the latest Neoproterozoic.
359 The large accumulation of organic matter associated with decaying animal carcasses
360 provides a local source for anaerobic degradation processes that can cause focused
361 alkalinity increase and thus facilitate carbonate formation (e.g., Duck, 1995). Inorganic
362 mineral phases (shell calcite, aragonite, or phosphate and bone) can also provide
363 nucleation sites for precipitation due in part to the reduced thermodynamic hurdles
364 related to mineral formation on preexisting crystalline materials (Berner, 1980;
365 Sunagawa, 1994).

366 The arrival of extensive (plant) terrestrial ecosystems during the Silurian
367 (Supplementary Figure 5) and their expansion thereafter (Gibling and Davies, 2012;

368 Kenrick and Crane, 1997) likely resulted in a more substantial delivery of exogenous
369 organic matter to the oceans. Such remains occur in marine sediments of the Phanerozoic
370 (Sackett et al., 1974). Raiswell and Berner (1986) have demonstrated a shift toward
371 higher C/S ratios in normal marine shales by the Middle Devonian, consistent with
372 increased delivery of terrestrial organic matter (TOM) thereafter. Remineralization of this
373 TOM could promote carbonate concretion authigenesis. Indeed, modern TOM is thought
374 to provide a significant portion of the total organic carbon budget, particularly in coastal
375 marine sediments (Burdige, 2005; Schlünz and Schneider, 2000). However, TOM may be
376 less reactive than marine organic matter (Aller et al., 1996; Burdige, 2005; Hedges et al.,
377 1997), potentially obscuring the potential impacts of increased delivery. Regardless, such
378 a fundamental shift in carbon sources to marine sediments is likely to have impacted
379 shallow marine diagenetic processes in shelf and slope depositional settings.
380
381 **4.3. Oxidant availability and its influence on organic matter remineralization**
382 Diagenetic processes in shallow marine sediments (including concretion
383 formation) are impacted by the abundance of organic carbon (Arndt et al., 2013), the
384 availability and nature of which has likely changed through geologic time (see above).
385 Remineralization reactions may or may not require additional external oxidant and thus
386 the fate of buried organic matter is variably tied to oxidant availability. The temporal
387 variability of select oxidants, including sedimentary iron oxide and marine sulfate
388 contents (recognized as important in organic matter remineralization and carbonate
389 authigenesis) is discussed in this section.

The idea that Earth's surface has experienced progressive oxygenation is widely accepted. The structure of this oxygenation however, remains a topic of considerable debate. In addition, progressive oxygenation likely impacted the abundances of specific oxidants through time differently. These oxidant budgets in turn likely imparted a first-order control on sedimentary diagenesis of marine environments by stimulating oxidative degradation of organic matter and methane. The temporal evolutions of oxygen and oxidant availability are outlined below.

4.3.1 Oxygen (O_2)

Atmospheric oxygen concentrations likely provide a first-order control on the oxidation state and oxidant capacity of surface environments (both terrestrial and marine). The oxygen content of the atmosphere is thought to have increased as a result of two major oxygenation events. The first of these corresponds to the ~2.5–2.3 Ga Great Oxidation Event (GOE) and is at least casually linked to photosynthetic O_2 buildup (Holland, 2002). This earlier oxygen increase, however, was probably not permanent, terminating with a return to lower oxygen conditions (Bekker and Holland, 2012; Partin et al., 2013). The second increase in oxygen content is thought to have occurred during the Late Neoproterozoic to early Cambrian (Chen et al., 2015; Sahoo et al., 2012; Scott et al., 2008), may have resulted in the ventilation of portions of the deep ocean and heralded the oxygen-rich conditions exhibited today (Lyons et al., 2014). Phanerozoic atmospheric oxygen contents have also fluctuated, albeit at a higher level (between ~10-100% present atmospheric level) (e.g., Berner and Canfield, 1989; Lenton et al., 2018).

412 Despite increasing oxygen concentrations in Earth's atmosphere, the oxidation
413 state of the oceans has exhibited its own complexity, driven in part by the evolving
414 atmospheric boundary condition (Canfield, 1998; Lyons et al., 2009). Prior to the GOE
415 Earth's oceans were predominantly ferruginous (iron(II)-rich) at all depths. After the
416 GOE and until the Proterozoic-Phanerozoic boundary, the redox structure shifted to
417 include oxic and/or sulfidic shallow/mid-depth waters over a persistently ferruginous
418 deep ocean, reflecting in part the delivery of sulfate by oxidative weathering on land and
419 its subsequent reduction to hydrogen sulfide in the water column (Lyons et al., 2009;
420 Planavsky et al., 2011; Poulton et al., 2010). In contrast, generally oxygenated oceans
421 typify the Phanerozoic, with low oxygen and sulfidic marine environments restricted to
422 near-shore, productive and/or restricted settings (Anderson and Devol, 1973; Jacobs et
423 al., 1985; Price and Calvert, 1973; Skei, 1983). These marine transitions are relatively
424 coarse; the fine-scale structure of the redox state of the oceans is potentially much more
425 complex and remains the topic of considerable debate (Lyons et al., 2014). Although the
426 *general* transitions in atmospheric and ocean oxidation state are widely accepted, bottom
427 water concentrations of oxidized phases other than oxygen (including iron oxides and
428 dissolved sulfate) are less well constrained. Oxidant availability at the sediment–water
429 interface impacts the degradation potential of sedimentary organic matter and methane
430 and thus provides a first order control on shallow marine diagenesis.
431
432 4.3.2 Particulate Iron Oxide
433 Iron oxide minerals provide an attractive electron acceptor for organic matter and
434 methane oxidation and subsequent concretion precipitation. Iron reduction metabolisms

435 are thought to be relatively ancient, as indicated by iron isotope compositions in rocks as
436 old as ~3.8 Ga (Supplementary Figure 5) (Craddock and Dauphas, 2011). A compilation
437 of speciation data for shale-hosted iron provides insight into the relative availability of
438 iron oxide through time (Figure 6). The highly reactive iron fraction (FeHR) includes
439 oxide phases (e.g., hematite, magnetite) and reduced phases (e.g., pyrite and iron
440 carbonate minerals) (Raiswell and Canfield, 1998) and thus can be used to assess the
441 original iron oxide content (before and after reduction) of marine sediments (see below).
442 Despite changes in the oxidation state of Earth's surface, broadly expressed as an
443 increase in atmospheric and oceanic oxygen through time, the availability of FeHR in
444 marine shale appears relatively static (Figure 6). Indeed, Sperling et al. (2015) find
445 similarly unchanged iron speciation from the Proterozoic to the early Paleozoic. Iron data
446 have also been screened to exclude samples with FeHR/FeT values greater than 0.38 (the
447 threshold for sediments deposited under anoxic conditions; Poulton and Raiswell, 2002),
448 to remove samples with elevated FeHR that are unrelated to sedimentary Fe^{3+} delivery.
449 This restricted data set likewise does not show significant variability among the time
450 intervals of interest here. However, iron speciation data are not equally available for the
451 different time periods (Sperling et al., 2015). More continuous population of this data set
452 may reveal temporal variability that is missed by this compilation.
453
454 4.3.3 Aqueous Sulfate
455 The understanding of the temporal evolution of marine sulfate concentrations has
456 developed significantly over the past twenty years. This understanding stems from fluid
457 inclusion data (Horita et al., 2002; Lowenstein et al., 2003), sulfur isotope variability

458 (Algeo et al., 2015; Gill et al., 2011; Kah et al., 2004; LaFlamme et al., 2021; Planavsky
459 et al., 2012) and fractionation magnitude experiments (Habicht et al., 2002), modeling
460 (Berner, 2004; Fakhraee et al., 2018; Fakhraee et al., 2019; Krause et al., 2022; Shi et al.,
461 2022) and the occurrence of marine evaporite deposits in the geologic record (Evans,
462 2006; Halevy et al., 2012; Wortmann and Chernyavsky, 2007). Sulfate concentrations
463 (Figure 7) exhibit a transient rise in association with the ~2.3 to 2.1 Ga Lomagundi
464 interval (Planavsky et al., 2012; Salop, 1982; Schröder et al., 2008) which overlaps with
465 the beginning of the relatively concretion-abundant interval at ~2.15 to 1.75 Ga
466 (Melezhik and Fallick, 1996). Evaporite paragenetic data that show halite saturation prior
467 to gypsum/anhydrite may indicate a return to low sulfate concentrations by ~1.9 Ga
468 (Blättler et al., 2018; Pope and Grotzinger, 2003).
469 At ~1.7 Ga sulfate concentrations have been estimated at ~1.5 mM and remain
470 below ~5 mM until ~750 Ma where sulfate concentrations increase to ~10 ± 5 mM
471 (Blättler et al., 2020; Kah et al., 2004; Krause et al., 2022), similar to the Phanerozoic
472 minimum (Horita et al., 2002; Lowenstein et al., 2003). Within the Phanerozoic, sulfate
473 concentrations vary (Figure 7b), reaching up to ~28 mM in the modern (Horita et al.,
474 2002; Lowenstein et al., 2003). This variability is broadly characterized by two stepwise
475 increases, one occurring across the Ediacaran–Cambrian boundary where concentrations
476 are thought to have reached up to ~10 mM in the early Cambrian and the other beginning
477 in the late Paleozoic. The timing of late Paleozoic sulfate increase varies depending on
478 literature source; however most reconstructions display an increase at the beginning or
479 within the Carboniferous. Note that the sulfate records presented in Figure 7 may not
480 include brief episodes of sulfate fluctuation such as those associated with the Permian–

Triassic interval (Luo et al., 2010; Song et al., 2014) and Cretaceous Ocean Anoxic Events (Adams et al., 2010; Ohkouchi et al., 1999).

4.4. Evolving carbon isotope distribution in shallow diagenetic environments throughout Earth history

As discussed above, $\Delta^{13}C_{con\text{-}sw}$ provides insights into temporal changes in shallow marine diagenesis, particularly when isotope compositions exceed or fall below threshold values. Data mean, maximum, minimum and range values for different age intervals demonstrate significant temporal variability (Figure 4), perhaps related to evolving marine diagenetic environments. It is important to note that the data-limited Neoproterozoic and older record may be more susceptible to biases associated with local rather than global environmental controls (depositional environment, etc.) compared to the data-replete younger record. We acknowledge that additional data collection may help resolve this potential bias and interpret the concretion carbon isotope variability demonstrated here in the context of broad temporal changes in Earth's surface environment. A lack of clear changes in reactive/oxide iron phases (Figure 6, Supplementary Figure 6) suggests that particulate iron oxides do not drive $\Delta^{13}C_{con\text{-}sw}$ variability. Thus, concretion isotope evolution is discussed in the context of other potential controls in the following discussion.

Prior to ~2.15 Ga, concretions yield values that overlap with or exceed contemporaneous seawater values (i.e., $\Delta^{13}C_{con\text{-}sw} \geq 0‰$, Figure 3). The earliest concretions (~2.8 Ga) express positive $\Delta^{13}C_{con\text{-}sw}$ values indicating formation as a result of methanogenesis (Dix et al., 1995). Molecular clock studies suggest early evolution of

504 methanogenesis metabolisms, perhaps originating at ~3.8 to 4.1 Ga (Supplementary
505 Figure 5) (Battistuzzi et al., 2004), well before the formation of these earliest known
506 concretions. Later Archean concretions within ~2.6 Ga rocks express $\delta^{13}C$ values that do
507 not differ significantly from seawater values (Figure 3a), suggesting a dominantly marine
508 DIC or primary carbonate mineral dissolution source.

509 The prevalence of near neutral $\Delta^{13}C_{con\text{-}sw}$ values during the Precambrian (Figure
510 3) may reflect the combined effects of low sulfate availability and high marine DIC
511 contents. As confirmed by model results, lower sulfate concentrations limit porewater
512 oxidation of sedimentary organic matter and methane and preclude severe decreases in
513 $\delta^{13}C_{DIC}$ (Figure 8 and Supplementary Figure 7) and thus $\Delta^{13}C_{con\text{-}sw}$. This is consistent
514 with previous modelling work exploring impacts of low sulfate concentration on
515 porewater and authigenic carbonate $\delta^{13}C$ (Laakso and Schrag, 2020). Marine DIC
516 contents may have been relatively high early in Earth history as supported by muted
517 variability in marine $\delta^{13}C$ (Bartley and Kah, 2004) and carbonate fabrics that indicate
518 rapid precipitation (Grotzinger and James, 2000). Under elevated marine DIC conditions,
519 shallow porewaters would be buffered against isotope modification by diagenesis. The
520 potential impacts of an increased marine DIC reservoir are demonstrated in Figure 9.
521 Importantly, under low sulfate and high marine DIC conditions, porewater $\delta^{13}C_{DIC}$
522 variability is diminished, manifested primarily as an increase in minimum values. Under
523 higher sulfate concentrations, the impacts of increasing marine DIC are less substantial.
524 Therefore, high marine DIC values during the Precambrian may have contributed to the
525 limited variability observed in $\Delta^{13}C_{con\text{-}sw}$.

Conclusively oxidation-derived carbonate concretions first appear at ~2.15 Ga. In fact, all concretion-hosting units between ~2.15 and 1.75 Ga include samples with predominantly negative $\Delta^{13}C_{con\text{-}sw}$ (Figure 3a). The $\Delta^{13}C_{con\text{-}sw}$ values extend down to ~ –25‰, consistent with at least partial carbon incorporation from organic matter, methane or both (Melezhik and Fallick, 1996). The $\Delta^{13}C_{con\text{-}sw}$ value of Lomagundi concretions (and other Precambrian-aged concretions) is constrained by nearby limestones considered to reflect primary marine DIC (see Results). In this regard, the ^{13}C-depleted $\Delta^{13}C_{con\text{-}sw}$ values of the Lomagundi interval should not be impacted by potential facies dependency of primary $\delta^{13}C$ values (Prave et al., 2022). In addition, the limestone $\delta^{13}C$ values used to constrain $\Delta^{13}C_{con\text{-}sw}$ do not exceed +5.4‰ (Supplementary Table 1) and thus do not drive the low $\Delta^{13}C_{con\text{-}sw}$ during this interval.

Intriguingly, the Lomagundi interval post-dates the GOE and coincides with a transient increase in marine sulfate concentration (Planavsky et al., 2012). Concretions of the Lomagundi interval express $\Delta^{13}C_{con\text{-}sw}$ values significantly lower than the preceding and following Precambrian (Figure 5), perhaps testament to a significant control of increased marine sulfate on porewater DIC (see Figure 8a). Concretions with the lowest $\Delta^{13}C_{con\text{-}sw}$ values formed during the highest marine sulfate concentrations (up to ~ 11 mM, Fakhraee et al., 2019; Planavsky et al., 2012) of the Lomagundi interval (Figure 7a). Thereafter, values increase but remain negative until ~1.75 Ga, despite an apparent massive drawdown in marine sulfate at the tail end of the Lomagundi event (Planavsky et al., 2012). Unfortunately, marine sulfate concentrations are not well resolved between the sulfate "crash" and ~1.75 Ga. Constraining sulfate concentrations in this interval would provide additional insight.

549 The next occurrence of carbonate concretions is reported in the ~1.4 Ga
550 Xiamaling Formation. These concretions express $\Delta^{13}C_{con\text{-}sw}$ near 0‰, interpreted to
551 represent a marine DIC carbon source (Liu et al., 2019) rather than one that requires
552 oxidative processes. Sulfate concentrations were relatively low at 1.4 Ga (Figure 7),
553 perhaps explaining the return to near neutral $\Delta^{13}C_{con\text{-}sw}$. The next youngest reported
554 concretions occur in shales of the ~745 Ma Kwagunt Formation of the Chuar Group
555 (Dehler et al., 2005). These concretions exhibit $\Delta^{13}C_{con\text{-}sw}$ values ranging from ~ –15 to ~
556 –7‰ (supplemented with new data reported here) and a return to at least partial carbon
557 derivation from the oxidation of organic matter and/or methane. Intriguingly, sulfate
558 concentrations may have been relatively high during this time interval (Kah et al., 2004),
559 which was followed by subsequent decreases associated with Neoproterozoic glacial
560 intervals (Hurtgen et al., 2002). Thus prior to the Cambrian, low $\Delta^{13}C_{con\text{-}sw}$ values
561 coincide with intervals of transient high marine sulfate concentrations.
562 Negative $\Delta^{13}C_{con\text{-}sw}$ values dominate the relatively well-resolved Phanerozoic
563 record thereafter (Figure 3), when marine sulfate concentrations were high. Indeed, mean
564 $\Delta^{13}C_{con\text{-}sw}$ values are significantly lower in the Phanerozoic compared to non-Lomagundi
565 Precambrian counterparts (Figure 4a). Phanerozoic mean $\Delta^{13}C_{con\text{-}sw}$ values range from ~ –
566 7.9 to –5.6‰ whereas the non-Lomagundi Precambrian mean $\Delta^{13}C_{con\text{-}sw}$ value is ~ –0.5‰
567 (Figure 4). This decrease demonstrates the oxidative impact of a growing marine sulfate
568 reservoir. Intriguingly, the mean $\Delta^{13}C_{con\text{-}sw}$ value remains relatively stable throughout the
569 Phanerozoic, despite a subsequent increase in marine sulfate during the mid- to late
570 Paleozoic. The static Phanerozoic mean $\Delta^{13}C_{con\text{-}sw}$ values developed, in part, as a result of
571 the expansion of the concretion carbon isotope record to include compositions both

572 depleted and enriched in ^{13}C (Figure 4). The implications of this expansion as related to
573 changing minimum and maximum $\Delta^{13}C_{con\text{-}sw}$ are discussed below.

574 Early Paleozoic concretions (Cambrian to Devonian samples) express a minimum
575 $\Delta^{13}C_{con\text{-}sw}$ value that extends down to ~ –25‰, the approximate concurrent organic matter
576 composition. This minimum value is similar to that of the Lomagundi interval (Figure 4,
577 Supplementary Table 5). Reported marine sulfate concentrations are comparable for these
578 two time intervals, reaching up to ~10 mM (Figure 7). This similarity underscores the
579 control of marine sulfate concentrations on $\Delta^{13}C_{con\text{-}sw}$.

580 $\Delta^{13}C_{con\text{-}sw}$ values do not drop below –25‰ until ~325 Ma (Figures 3 and 4),
581 following reported elevated marine sulfate concentrations in the Carboniferous (Berner,
582 2004; Gill et al., 2007; Halevy et al., 2010) and representing the first conclusive evidence
583 for methane oxidation-derived inorganic carbon. Similar low isotope compositions persist
584 throughout the remaining record (see minimum $\Delta^{13}C_{con\text{-}sw}$ values in Figure 4). These data
585 imply that the AOM pathway has been an important methane consumption and
586 concretion producing reaction since at least ~325 Ma and perhaps earlier (methane
587 oxidation-derived concretions need not produce values below –25‰ if other carbon
588 sources also contributed). Modern marine sediments often show porewater $\delta^{13}C_{DIC}$
589 minima that approach but do not drop below the organic matter value despite active
590 AOM, suggesting quantitative oxidation of locally produced methane by sulfate in
591 shallower sediments (Meister et al., 2019). Modeling results indicate that both high
592 marine sulfate and an external source of methane are required to produce isotope
593 compositions significantly lower than –25‰ (Figure 8 and Supplementary Figure 7). The
594 degree of ^{13}C depletion below –25‰ ultimately depends on marine sulfate content, the

595 amount of methane entering the system and its $\delta^{13}C$. Perhaps not surprisingly, non-
596 concretionary methane cold-seep authigenic carbonates express similarly diagnostic, low
597 $\delta^{13}C$ values at about the same time. The transition to conclusively methane-oxidation-
598 derived seep carbonates has likewise been attributed to increased marine sulfate
599 concentrations (Bristow and Grotzinger, 2013). The Paleozoic appearance of
600 diagnostically low concretion and seep-carbonate $\Delta^{13}C_{con\text{-}sw}$ values did not result from the
601 concurrent evolution of organisms capable of AOM as these lineages are relatively
602 ancient, perhaps existing since ~2.6 to 2.8 Ga (Supplementary Figure 5) (Battistuzzi et
603 al., 2004; Hinrichs, 2002).
604 The relationship of AOM-derived authigenic carbonate to temporal delivery of
605 external methane is more difficult to resolve. We speculate that the generation of
606 significant methane accumulations may in part be related to enhanced organic carbon
607 burial in the Phanerozoic (from marine and/or terrestrial sources, see above). This
608 methane could then be delivered to shallow sediments relatively quickly (perhaps through
609 methane hydrate dissolution, for example) and oxidized to generate the severe ^{13}C
610 depletions diagnostic of AOM. A negative correlation between mean organic carbon
611 burial rates and minimum $\Delta^{13}C_{con\text{-}sw}$ values (that also drop below –25‰, Figure 10)
612 supports this assertion. Constraining the temporal distribution of large methane reserves
613 is beyond the scope of this work, but may provide additional insight.
614
615 **4.5. Identifying dominant controls on carbon isotope minima and maxima of**
616 **inorganic carbon**
617

618 *4.5.1. $\delta^{13}C$ minima in the AOM zone*

619 As discussed above, sulfate appears to play an integral role in governing Earth's
620 shallow marine digenetic environments. The relationship between marine sulfate
621 concentration and concretion isotope compositions is emphasized in Figure 8d. This plot
622 demonstrates a strong negative correlation between the sulfate content and minimum
623 $\Delta^{13}C_{con\text{-}sw}$ during the time intervals discussed above. Encouragingly, this correlation
624 mimics the porewater minimum $\delta^{13}C_{DIC}$ model results of Figure 8c where the impacts of
625 changing marine sulfate contents are displayed under variable external methane flux.
626 Ultimately these results demonstrate that marine sulfate concentrations and the delivery
627 of external methane dictate the minimum $\delta^{13}C_{DIC}$ (and $\Delta^{13}C_{con\text{-}sw}$) values generated in the
628 AOM zone.

629

630 *4.5.2. $\delta^{13}C$ maxima in the methanogenic zone*

631 Collectively, Phanerozoic concretions express $\Delta^{13}C_{con\text{-}sw}$ values that are consistent
632 with oxidation and methane-producing reactions. The increase in the range in isotope
633 compositions within the Phanerozoic is manifested as both a decrease in minimum and an
634 increase in maximum values (Figures 3 and 4). As discussed above, sulfate appears to be
635 an important external oxidant as revealed by relationships between sulfate concentration
636 and $\Delta^{13}C_{con\text{-}sw}$ data. However, the coincident increase in the abundance of conclusively
637 methanogenesis-derived concretions (as indicated by positive $\Delta^{13}C_{con\text{-}sw}$) is not
638 straightforwardly attributable to increasing sulfate concentrations.

639 It has been proposed that an increase in the quantity of organic matter delivered to
640 the sediment-water interface may dictate the relative importance of concretion-yielding

641 diagenetic reactions, such that higher amounts promote organic matter persistence to the
642 deeper methanogenesis zone (Mozley and Burns, 1993). In this regard, the increase in the
643 quantity of organic matter in Phanerozoic compared to Neoproterozoic marine sediments
644 recognized by Sperling and Stockey (2018) and supported by model reconstructions
645 (Krause et al., 2022; Krissansen‐Totton et al., 2021; Planavsky et al., 2022) may have
646 promoted the expansion of methanogenesis (Sivan et al., 2007). However, maximum
647 $\Delta^{13}C_{con\text{-}sw}$ values do not show significant correlation with organic carbon burial (Figure
648 11a). Figure 11b and Supplementary Figure 8 show variability in modeled maximum
649 $\delta^{13}C_{DIC}$ values as a function of TOC deposited at the seafloor. Note that the global
650 organic carbon burial rate does not dictate the specific quantity of TOC deposited on the
651 seafloor at any given location. However, broad increases in organic carbon burial are
652 likely to lead to generally higher TOC delivery globally, explaining the motivation
653 behind panel comparisons in Figure 11. As initial TOC increases so does the maximum
654 $\delta^{13}C_{DIC}$; however isotope compositions do not exceed ~ +15‰ (Figure 12b,
655 Supplementary Figure 8). Meister et al. (2019) demonstrate this maximum threshold
656 under modern marine sulfate concentrations (28 mM) and new model results show that
657 lower sulfate concentrations do not significantly increase $\delta^{13}C_{DIC}$ maximum values. Thus
658 the $\Delta^{13}C_{con\text{-}sw}$ values above ~ +20‰ commonly expressed in the Phanerozoic record
659 cannot be accounted for by organic carbon burial alone.
660 It has been demonstrated that increased sedimentation rates lead to faster organic
661 matter burial and degradation in the deeper methanogenesis zone (Burns and Baker,
662 1987; Pisciotto and Mahoney, 1981; Scotchman, 1991), largely due to limitations

663 associated with sulfate diffusion from the overlying water column. As yet, no data have
664 been reported that indicate an increased sedimentation rate in the Phanerozoic
665 compared to earlier times. Organic matter reactivity can also impact degradation
666 mechanisms. Similar to increased sedimentation rate, less reactive organic matter
667 degrades more slowly and can persist to deeper sediment depths to experience
668 preferential degradation in the methanogenesis zone (Meister et al., 2019). Thus, higher
669 proportions of more refractory organic matter can cause porewater DIC to become more
670 ^{13}C-enriched with depth. The evolution of organic matter reactivity is not well known,
671 but the arrival and diversification of terrestrial plants may have prompted the delivery of
672 less reactive organic material (Aller et al., 1996; Burdige, 2005; Hedges et al., 1997) to
673 marginal environments since the Silurian (Kenrick and Crane, 1997; Raiswell and
674 Berner, 1986). Maximum $\Delta^{13}C_{con\text{-}sw}$ values, however, show an increase well before the
675 appearance of land plants (Supplementary Figure 5). Furthermore, significant decreases
676 in organic matter degradation rate are unable to account for porewater DIC ^{13}C
677 enrichments above ~ +10‰ in the methanogenesis zone (Meister et al., 2019) like those
678 expressed in the concretion record. Whereas sedimentation rate and organic matter
679 quantity and reactivity may impact organic matter degradation mechanisms, these factors
680 alone cannot explain the observed data.

681 Another more speculative explanation involves an increase in the magnitude of
682 carbon isotope fractionation during methanogenesis. Fractionation factors between
683 methane and DIC ($\alpha_{methane\text{-}DIC}$) determined from culture and modern porewater data are
684 between 0.95 and 1.0 (Londry et al., 2008; Whiticar et al., 1986). Some modern marine
685 sediments, however, express $\delta^{13}C_{DIC}$ maxima that are difficult to reconcile with low

686 fractionation magnitudes (Meister et al., 2019). In addition, the concretion record
687 suggests that higher maximum porewater $\delta^{13}C_{DIC}$ compositions occurred in more recent
688 marine sediments, exceeding the values that can be reached by using the experimentally
689 determined fractionation factors mentioned above. It has been suggested that substrate
690 limitation during AOM promotes reaction reversibility as part of the Wood-Ljungdahl
691 pathway and that this reversibility can lead to isotopic fractionation that approaches
692 theoretical equilibrium magnitudes (Yoshinaga et al., 2014). Similar reversibility may
693 affect isotope fractionation during methanogenesis as suggested by some culture
694 experiments conducted under substrate limited conditions (Botz et al., 1996 ; see
695 comparison in Meister and Reyes (2019)) and isotope separations between co-occurring
696 porewater DIC and methane recognized in porewaters of many marine sediments
697 (e.g.,(Galimov and Kvenvolden, 1983; Heuer et al., 2009; Meister et al., 2019; Paull et
698 al., 2000; Pohlman et al., 2008) . It is conceivable that under extreme substrate limitation
699 (which is common in sub-seafloor environments) the fractionation factor may approach
700 the theoretical low-temperature equilibrium value ($\alpha_{methane\text{-}DIC}$ = 0.93,(Bottinga, 1969);
701 Horita (2001)).

702 To explore the effect of the fractionation factor on maximum $\delta^{13}C_{DIC}$, model
703 experiments were conducted at variable $\alpha_{methane\text{-}DIC}$ (from 0.92 to 0.98, Supplementary
704 Figures 9 and 10). In these experiments, methane was sourced entirely from within the
705 model domain (i.e., no external methane flux imposed). Maximum $\delta^{13}C_{DIC}$ values
706 increased at lower fractionation factors, reaching up to ~ +9‰ (at $\alpha_{methane\text{-}DIC}$ = 0.92).
707 However, in this most extreme scenario the isotopic separation between methane and
708 DIC becomes very high (~ 100‰) and exceeds differences commonly observed in

709 measured profiles. Increasing the external methane flux did not significantly change
710 maximum $\delta^{13}C_{DIC}$ when external methane was assigned the $\delta^{13}C$ composition of the in-
711 situ methane produced at the bottom of the model domain (Supplementary Figures 9 and
712 10). Thus, increased isotope fractionation alone cannot account for the highly positive
713 $\Delta^{13}C_{con\text{-}sw}$ values expressed in the concretion record.

714 One mechanism that could promote extreme ^{13}C enrichment of porewater DIC
715 involves equilibration with externally derived methane exhibiting a relatively high $\delta^{13}C$.
716 Such methane can form through thermogenic processes and exhibit isotope compositions
717 near ~ –40‰. Hypothetically, equilibration between thermogenic methane and DIC could
718 result in $\delta^{13}C_{DIC}$ values up to ~ +30 to +40‰ if the methanogenic reaction is reversible
719 (such that isotope exchange occurs between methane and DIC) and an isotope offset of
720 ~70 to 80‰ is maintained. Such a process may in part explain the very high $\delta^{13}C_{DIC}$
721 values recognized at some Cascadia Margin sites (Heuer et al., 2009), although other
722 factors including gas escape to the water column may also play a role (Birgel et al., 2015;
723 Meister et al., 2019). Despite the poorly understood complexities involved in isotope
724 fractionation during methanogenesis and the potential role of equilibration, the
725 mechanisms of ^{13}C enrichments and depletions in porewater DIC may both involve the
726 influx of external methane. As argued above, methane formation (thermogenic or
727 biogenic) may have been stimulated as a result of enhanced organic carbon burial during
728 the Phanerozoic, thus providing a singular driver for the roughly contemporaneous
729 expansion in $\Delta^{13}C_{con\text{-}sw}$ range.

730

731 **4.6. Implications for the $\delta^{13}C$ of authigenic carbonate**

732 Modern authigenic carbonates form within marine sediments as a result of similar
733 reactions to those proposed for carbonate concretions. In fact, carbonate concretions are
734 thought to represent ancient analogs to modern authigenic carbonates (Loyd and
735 Berelson, 2016). This connection has been confounded in part as a result of the inability
736 to identify core-recovered carbonate as concretionary in nature (core sampling limits the
737 ability to characterize the three-dimensional structure of large objects). The similarity
738 between the carbon isotope composition of authigenic carbonate ($\delta^{13}C_{auth}$) and Triassic to
739 Holocene $\Delta^{13}C_{con\text{-}sw}$ values (Figure 4) provides further support to the proposed analogy.
740 Thus, the concretion-based record presented here may provide insight into the evolution
741 of $\delta^{13}C_{auth}$ through time.

742 As with the carbon isotope composition of carbonate concretions, $\delta^{13}C_{auth}$ is likely
743 to have changed as a result of broad changes in the oxidation state of marine bottom
744 waters. Previous work aimed at exploring the impact of authigenic carbonate
745 precipitation on global carbon budgets and marine $\delta^{13}C_{DIC}$ hinges intimately on
746 constraining an average $\delta^{13}C_{auth}$ value (Schrag et al., 2013). Indeed, Schrag et al. (2013)
747 and Laakso and Schrag (2020) propose that average $\delta^{13}C_{auth}$ values may have been
748 different in the past and this inference is supported by the Precambrian $\Delta^{13}C_{con\text{-}sw}$ record.
749 When data outside the Lomagundi interval are considered, mean Precambrian $\Delta^{13}C_{con\text{-}sw}$
750 values differ significantly from other time intervals (Figure 4). The average Precambrian
751 non-Lomagundi $\Delta^{13}C_{con\text{-}sw}$ value is very near neutral (~ –0.5‰) and indistinguishable
752 from contemporaneous primary carbonate. Therefore, according to this concretion data
753 set, burial of Precambrian authigenic carbonate would have had little impact on marine
754 $\delta^{13}C$ variability. Once marine sulfate concentrations exceeded ~ 5 mM (during brief

755 transient intervals in the Precambrian or otherwise), mean $\Delta^{13}C_{con\text{-}sw}$ values consistently
756 lie between ~ −10 and ~ −5‰. These compositions agree with recent findings of Laakso
757 and Schrag (2020), are comparable to, to somewhat higher than approximate $\delta^{13}C_{auth}$
758 values proposed by Schrag et al. (2013), and considerably higher than the estimated
759 modern average $\delta^{13}C_{auth}$ value of – 20.5 +/– 3.5‰, based on compiled pore water
760 geochemical data (Bradbury and Turchyn, 2019). Differences in mean values may in part
761 be explained by the exclusion of non-concretionary, seafloor methane seep carbonates
762 and/or preferential retention of methanogenesis-formed carbonate in the sampled
763 concretion record.
764
765 **5. CONCLUSIONS**
766 Carbonate concretions primarily occur in Phanerozoic rock units and a
767 concretion-rich interval between ~2.15 and 1.75 Ga that overlaps with the enigmatic
768 Lomagundi carbon isotope excursion (Melezhik and Fallick, 1996). This distribution may
769 result from preferential formation during these time intervals, but correlation with the
770 abundance of preserved sedimentary rock precludes identification of an environmental
771 signal in the concretion occurrence record. In contrast, the concretion isotope record
772 provides important information about shallow marine diagenetic environments. Negative
773 $\Delta^{13}C_{con\text{-}sw}$ values dominate the Phanerozoic and Lomagundi interval and correlate with
774 periods exhibiting high marine dissolved sulfate concentrations and organic carbon burial
775 rates. Concretions with conclusively AOM carbon isotope signals appear at ~325 Ma and
776 are relatively common in the younger record, likely in response to a Paleozoic rise in
777 marine sulfate concentrations and significant delivery of external methane. The

Phanerozoic record also shows an increase in $\Delta^{13}C_{con\text{-}sw}$ through time perhaps resulting from increased input of thermogenic methane and isotopic equilibration with porewater DIC. Ultimately, the concretion record demonstrates coeval evolution of Earth's primary marine and shallow diagenetic environments, in part related to shifting redox conditions.

Acknowledgements

We thank Julie Unson and Miguel Rincon for analytical assistance and Mary Droser for providing Chuar Group samples. Jon Husson provided integral rock abundance data from the Macrostrat database. Insightful communications with Peter Mozley, Doug LaRowe, Kristen Bergmann, Eric Sperling, Maggie Osborn and David Ware and early reviews provided by Ben Gill, Leanne Hancock and one anonymous reviewer were highly beneficial to this manuscript.

Funding: This research was funded in part by CSUF 2016-17 Incentive, CSUF 2018-19 JrSr and CSUF 2019 RSCA grants awarded to SJL. BL funded by the BMBF MARE:N project "Anthropogenic impacts on particulate organic carbon cycling in the North Sea (APOC)" (03F0874C).

Appendix A. Supplementary Material

Supplementary material related to this manuscript includes tabulated concretion and modern authigenic carbonate data, statistical analysis results, a description of the applied reaction transport model, histograms of $\Delta^{13}C_{con\text{-}sw}$ data at different time intervals, the temporal trend of $\Delta^{13}C_{con\text{-}sw}$ with samples grouped according to $\delta^{18}O_{con}$ (where available), comparison between the concretion abundance record and the preservation of marine sedimentary rock, the temporal trend of $\Delta^{13}C_{con\text{-}sw}$ maxima, mean and minima alongside major evolutionary events, comparison of the temporal trend of $\Delta^{13}C_{con\text{-}sw}$ maxima, mean and minima with iron speciation data and select reaction transport model results. Supplementary data to this article can be found online at XXX.

References

Adams, D.D., Hurtgen, M.T., Sageman, B.B., 2010. Volcanic triggering of a biogeochemical cascade during Oceanic Anoxic Event 2. Nature geoscience 3(3), 201-204.

Algeo, T., Luo, G., Song, H., Lyons, T., Canfield, D., 2015. Reconstruction of secular variation in seawater sulfate concentrations. Biogeosciences 12(7), 2131-2151.

Aller, R., Blair, N., Xia, Q., Rude, P., 1996. Remineralization rates, recycling, and storage of carbon in Amazon shelf sediments. Continental Shelf Research 16(5-6), 753-786.

Allison, P.A., Pye, K., 1994. Early diagenetic mineralization and fossil preservation in modern carbonate concretions. Palaios 9, 561-575.

Anderson, J.J., Devol, A.H., 1973. Deep water renewal in Saanich Inlet, an intermittently anoxic basin. Estuarine and Coastal Marine Science 1(1), 1-10.

Arndt, S., Jørgensen, B.B., LaRowe, D.E., Middelburg, J., Pancost, R., Regnier, P., 2013. Quantifying the degradation of organic matter in marine sediments: A review and synthesis. Earth-science reviews 123, 53-86.

Bartley, J.K., Kah, L.C., 2004. Marine carbon reservoir, Corg-Ccarb coupling, and the evolution of the Proterozoic carbon cycle. Geology 32(2), 129. doi.org/10.1130/g19939.1.

Battistuzzi, F.U., Feijao, A., Hedges, S.B., 2004. A genomic timescale of prokaryote evolution: insights into the origin of methanogenesis, phototrophy, and the colonization of land. BMC evolutionary biology 4(1), 44.

Bekker, A., Holland, H., 2012. Oxygen overshoot and recovery during the early Paleoproterozoic. Earth and Planetary Science Letters 317, 295-304.

Berner, R.A., 1980. Early diagenesis: A theoretical approach. Princeton University Press.

Berner, R.A., 2004. A model for calcium, magnesium and sulfate in seawater over Phanerozoic time. American Journal of Science 304(5), 438-453.

Berner, R.A., Canfield, D.E., 1989. A new model for atmospheric oxygen over Phanerozoic time. American Journal of Science 289(4), 333-361.

Birgel, D., Meister, P., Lundberg, R., Horath, T., Bontognali, T.R., Bahniuk, A.M., de Rezende, C.E., Vásconcelos, C., McKenzie, J.A., 2015. Methanogenesis produces strong 13C enrichment in stromatolites of Lagoa Salgada, Brazil: a modern analogue for Palaeo‐/Neoproterozoic stromatolites? Geobiology 13(3), 245-266.

Bjørlykke, K., 1973. Origin of limestone nodules in the Lower Palaeozoic of the Oslo Region. Universitetsforlaget.

Blättler, C., Claire, M., Prave, A.R., Kirsimäe, K., Higgins, J., Medvedev, P., Romashkin, A., Rychanchik, D., Zerkle, A.L., Paiste, K., 2018. Two-billion-year-old evaporites capture Earth's great oxidation. Science 360(6386), 320-323.

Blättler, C.L., Bergmann, K.D., Kah, L.C., Gómez-Pérez, I., Higgins, J.A., 2020. Constraints on Meso-to Neoproterozoic seawater from ancient evaporite deposits. Earth and Planetary Science Letters 532, 115951.

Blome, C.D., Albert, N.R., 1985. Carbonate concretions: An ideal sedimentary host for microfossils. Geology 13(3), 212-215.

Bojanowski, M.J., Barczuk, A., Wetzel, A., 2014. Deep‐burial alteration of early‐diagenetic carbonate concretions formed in Palaeozoic deep‐marine greywackes and mudstones (Bardo Unit, Sudetes Mountains, Poland). Sedimentology 61(5), 1211-1239.

Bottinga, Y., 1969. Calculated fractionation factors for carbon and hydrogen isotope exchange in the system calcite-carbon dioxide-graphite-methane-hydrogen-water vapor. Geochimica et Cosmochimica Acta 33(1), 49-64.
Botz, R., Pokojski, H.-D., Schmitt, M., Thomm, M., 1996. Carbon isotope fractionation during bacterial methanogenesis by CO2 reduction. Organic Geochemistry 25(3-4), 255-262.
Bradbury, H.J., Turchyn, A.V., 2019. Reevaluating the carbon sink due to sedimentary carbonate formation in modern marine sediments. Earth and Planetary Science Letters 519, 40-49.
Bradley, D.C., 2008. Passive margins through earth history. Earth-Science Reviews 91(1-4), 1-26.
Bramlette, M.N., 1946. The Monterey Formation of California and the origin of its siliceous rocks. US Government Printing Office, Washington.
Bristow, T.F., Grotzinger, J.P., 2013. Sulfate availability and the geological record of cold-seep deposits. Geology 41(7), 811-814. doi.org/10.1130/g34265.1.
Brocks, J.J., Jarrett, A.J., Sirantoine, E., Hallmann, C., Hoshino, Y., Liyanage, T., 2017. The rise of algae in Cryogenian oceans and the emergence of animals. Nature 548(7669), 578-581.
Burdige, D.J., 2005. Burial of terrestrial organic matter in marine sediments: A re‐assessment. Global Biogeochemical Cycles 19(4).
Burdige, D.J., 2007. Preservation of organic matter in marine sediments: controls, mechanisms, and an imbalance in sediment organic carbon budgets? Chemical reviews 107(2), 467-485.
Burns, S.J., Baker, P.A., 1987. A geochemical study of dolomite in the Monterey Formation, California. Journal of Sedimentary Research 57(1).
Canfield, D., 1998. A new model for Proterozoic ocean chemistry. Nature 396(6710), 450-453.
Chen, X., Ling, H.-F., Vance, D., Shields-Zhou, G.A., Zhu, M., Poulton, S.W., Och, L.M., Jiang, S.-Y., Li, D., Cremonese, L., 2015. Rise to modern levels of ocean oxygenation coincided with the Cambrian radiation of animals. Nature communications 6(1), 1-7.
Claypool, G.E., Kaplan, I., 1974. The origin and distribution of methane in marine sediments, Natural gases in marine sediments. Springer, New York, pp. 99-139.
Coleman, M.L., 1993. Microbial processes: controls on the shape and composition of carbonate concretions. Marine geology 113(1-2), 127-140.
Craddock, P.R., Dauphas, N., 2011. Iron and carbon isotope evidence for microbial iron respiration throughout the Archean. Earth and Planetary Science Letters 303(1-2), 121-132.
Dale, A., John, C.M., Mozley, P.S., Smalley, P., Muggeridge, A.H., 2014. Time-capsule concretions: unlocking burial diagenetic processes in the Mancos Shale using carbonate clumped isotopes. Earth and Planetary Science Letters 394, 30-37.
Dehler, C., Elrick, M., Bloch, J., Crossey, L., Karlstrom, K., Marais, D.D., 2005. High-resolution δ13C stratigraphy of the Chuar Group (ca. 770–742 Ma), Grand Canyon: Implications for mid-Neoproterozoic climate change. Geological Society of America Bulletin 117(1-2), 32-45.

Derry, L.A., Kaufman, A.J., Jacobsen, S.B., 1992. Sedimentary cycling and environmental change in the Late Proterozoic: evidence from stable and radiogenic isotopes. Geochimica et Cosmochimica Acta 56(3), 1317-1329.
Des Marais, D.J., Strauss, H., Summons, R.E., Hayes, J., 1992. Carbon isotope evidence for the stepwise oxidation of the Proterozoic environment. Nature 359(6396), 605-609.
Dix, G.R., Thomson, M.L., Longstaffe, F.J., McNutt, R.H., 1995. Systematic decrease of high δ13C values with burial in late Archaean (2.8 Ga) diagenetic dolomite: evidence for methanogenesis from the Crixás Greenstone Belt, Brazil. Precambrian Research 70(3-4), 253-268.
Duck, R., 1995. Subaqueous shrinkage cracks and early sediment fabrics preserved in Pleistocene calcareous concretions. Journal of the Geological Society 152(1), 151-156.
Efron, B., 1979. Bootstrap methods: Another look at the jackknife. Annals of Statistics 7, 1-26.
Efron, B., 1982. The jackknife, the bootstrap and other resampling plans. SIAM, Philadelphia PA.
Eguchi, J., Seales, J., Dasgupta, R., 2020. Great Oxidation and Lomagundi events linked by deep cycling and enhanced degassing of carbon. Nature geoscience 13(1), 71-76.
El Albani, A., Vachard, D., Kuhnt, W., Thurow, J., 2001. The role of diagenetic carbonate concretions in the preservation of the original sedimentary record. Sedimentology 48(4), 875-886.
Emrich, K., Ehhalt, D., Vogel, J., 1970. Carbon isotope fractionation during the precipitation of calcium carbonate. Earth and Planetary Science Letters 8(5), 363-371.
Evans, D.A., 2006. Proterozoic low orbital obliquity and axial-dipolar geomagnetic field from evaporite palaeolatitudes. Nature 444(7115), 51-55.
Fakhraee, M., Crowe, S.A., Katsev, S., 2018. Sedimentary sulfur isotopes and Neoarchean ocean oxygenation. Science advances 4(1), e1701835.
Fakhraee, M., Hancisse, O., Canfield, D.E., Crowe, S.A., Katsev, S., 2019. Proterozoic seawater sulfate scarcity and the evolution of ocean–atmosphere chemistry. Nature Geoscience 12(5), 375-380.
Gaines, R.R., Kennedy, M.J., Droser, M.L., 2005. A new hypothesis for organic preservation of Burgess Shale taxa in the middle Cambrian Wheeler Formation, House Range, Utah. Palaeogeography, Palaeoclimatology, Palaeoecology 220(1-2), 193-205. doi.org/10.1016/j.palaeo.2004.07.034.
Galimov, E., Kvenvolden, K.A., 1983. Concentrations and carbon isotopic compositions of CH4 and CO2 in gas from sediments of the Blake Outer Ridge, Deep Sea Drilling Project Leg 76. Initial Reports of the DSDP 76, 403-407.
Gibling, M.R., Davies, N.S., 2012. Palaeozoic landscapes shaped by plant evolution. Nature Geoscience 5(2), 99-105.
Gill, B.C., Lyons, T.W., Saltzman, M.R., 2007. Parallel, high-resolution carbon and sulfur isotope records of the evolving Paleozoic marine sulfur reservoir. Palaeogeography, Palaeoclimatology, Palaeoecology 256(3-4), 156-173.
Gill, B.C., Lyons, T.W., Young, S.A., Kump, L.R., Knoll, A.H., Saltzman, M.R., 2011. Geochemical evidence for widespread euxinia in the later Cambrian ocean. Nature 469(7328), 80-83. doi.org/10.1038/nature09700.
Gross, M.G., Tracey Jr, J.I., 1966. Oxygen and carbon isotopic composition of limestones and dolomites, Bikini and Eniwetok Atolls. Science 151(3714), 1082-1084.

Grotzinger, J.P., James, N.P., 2000. Precambrian carbonates: evolution of understanding.
Habicht, K.S., Gade, M., Thamdrup, B., Berg, P., Canfield, D.E., 2002. Calibration of sulfate levels in the archean ocean. Science 298(5602), 2372-2374. doi.org/10.1126/science.1078265.
Halevy, I., Johnston, D.T., Schrag, D.P., 2010. Explaining the structure of the Archean mass-independent sulfur isotope record. Science 329(5988), 204-207. doi.org/10.1126/science.1190298.
Halevy, I., Peters, S.E., Fischer, W.W., 2012. Sulfate burial constraints on the Phanerozoic sulfur cycle. Science 337(6092), 331-334.
Halverson, G.P., Hoffman, P.F., Schrag, D.P., Maloof, A.C., Rice, A.H.N., 2005. Toward a Neoproterozoic composite carbon-isotope record. Geological Society of America Bulletin 117(9), 1181. doi.org/10.1130/b25630.1.
Hayes, J.M., Waldbauer, J.R., 2006. The carbon cycle and associated redox processes through time. Philosophical Transactions of the Royal Society B: Biological Sciences 361(1470), 931-950.
Hedges, J.I., Keil, R.G., Benner, R., 1997. What happens to terrestrial organic matter in the ocean? Organic geochemistry 27(5-6), 195-212.
Heimhofer, U., Meister, P., Bernasconi, S.M., Ariztegui, D., Martill, D.M., Rios‐Netto, A.M., Schwark, L., 2017. Isotope and elemental geochemistry of black shale‐hosted fossiliferous concretions from the Cretaceous Santana Formation fossil Lagerstätte (Brazil). Sedimentology 64(1), 150-167.
Hesselbo, S., Palmer, T., 1992. Reworked early diagenetic concretions and the bioerosional origin of a regional discontinuity within British Jurassic marine mudstones. Sedimentology 39(6), 1045-1065.
Heuer, V.B., Pohlman, J.W., Torres, M.E., Elvert, M., Hinrichs, K.-U., 2009. The stable carbon isotope biogeochemistry of acetate and other dissolved carbon species in deep subseafloor sediments at the northern Cascadia Margin. Geochimica et Cosmochimica Acta 73(11), 3323-3336.
Hinrichs, K.U., 2002. Microbial fixation of methane carbon at 2.7 Ga: Was an anaerobic mechanism possible? Geochemistry, geophysics, geosystems 3(7), 1-10.
Holland, H.D., 2002. Volcanic gases, black smokers, and the Great Oxidation Event. Geochimica et Cosmochimica acta 66(21), 3811-3826.
Horita, J., 2001. Carbon isotope exchange in the system CO2-CH4 at elevated temperatures. Geochimica et Cosmochimica Acta 65(12), 1907-1919.
Horita, J., Zimmermann, H., Holland, H.D., 2002. Chemical evolution of seawater during the Phanerozoic: Implications from the record of marine evaporites. Geochimica et Cosmochimica Acta 66(21), 3733-3756.
Hurtgen, M.T., Arthur, M.A., Suits, N.S., Kaufman, A.J., 2002. The sulfur isotopic composition of Neoproterozoic seawater sulfate: implications for a snowball Earth? Earth and Planetary Science Letters 203(1), 413-429.
Husson, J.M., Peters, S.E., 2018. Nature of the sedimentary rock record and its implications for Earth system evolution. Emerging Topics in Life Sciences 2(2), 125-136.
Irwin, H., Curtis, C., Coleman, M., 1977. Isotopic evidence for source of diagenetic carbonates formed during burial of organic-rich sediments. Nature 269, 209-213.

Jacobs, L., Emerson, S., Skei, J., 1985. Partitioning and transport of metals across the O2H2S interface in a permanently anoxic basin: Framvaren Fjord, Norway. Geochimica et Cosmochimica Acta 49(6), 1433-1444.
Kah, L.C., Lyons, T.W., Frank, T.D., 2004. Low marine sulphate and protracted oxygenation of the Proterozoic biosphere. Nature 431(7010), 834-838.
Karhu, J.A., Holland, H.D., 1996. Carbon isotopes and the rise of atmospheric oxygen. Geology 24(10), 867-870.
Keil, R.G., Montluçon, D.B., Prahl, F.G., Hedges, J.I., 1994. Sorptive preservation of labile organic matter in marine sediments. Nature 370(6490), 549-552.
Kennedy, M., Droser, M., Mayer, L.M., Pevear, D., Mrofka, D., 2006. Late Precambrian oxygenation; inception of the clay mineral factory. Science 311(5766), 1446-1449.
Kennedy, M.J., Pevear, D.R., Hill, R.J., 2002. Mineral surface control of organic carbon in black shale. Science 295(5555), 657-660.
Kenrick, P., Crane, P.R., 1997. The origin and early evolution of plants on land. Nature 389(6646), 33-39.
Kipp, M.A., Krissansen‐Totton, J., Catling, D.C., 2021. High organic burial efficiency is required to explain mass balance in Earth's early carbon cycle. Global Biogeochemical Cycles 35(2).
Knauth, L.P., Kennedy, M.J., 2009. The late Precambrian greening of the Earth. Nature 460(7256), 728-732. doi.org/10.1038/nature08213.
Koyama, T., 1963. Gaseous metabolism in lake sediments and paddy soils and the production of atmospheric methane and hydrogen. Journal of Geophysical Research 68(13), 3971-3973.
Krause, A.J., Mills, B.J., Merdith, A.S., Lenton, T.M., Poulton, S.W., 2022. Extreme variability in atmospheric oxygen levels in the late Precambrian. Science advances 8(41), eabm8191.
Krissansen‐Totton, J., Kipp, M.A., Catling, D.C., 2021. Carbon cycle inverse modeling suggests large changes in fractional organic burial are consistent with the carbon isotope record and may have contributed to the rise of oxygen. Geobiology 19(4), 342-363.
Kump, L.R., Arthur, M.A., 1999. Interpreting carbon-isotope excursions: carbonates and organic matter. Chemical Geology 161(1), 181-198.
Laakso, T.A., Schrag, D.P., 2020. The role of authigenic carbonate in Neoproterozoic carbon isotope excursions. Earth and Planetary Science Letters 549, 116534.
LaFlamme, C., Barré, G., Fiorentini, M.L., Beaudoin, G., Occhipinti, S., Bell, J., 2021. A significant seawater sulfate reservoir at 2.0 Ga determined from multiple sulfur isotope analyses of the Paleoproterozoic Degrussa Cu-Au volcanogenic massive sulfide deposit, Western Australia. Geochimica et Cosmochimica Acta 295, 178-193.
Lenton, T.M., Daines, S.J., Mills, B.J., 2018. COPSE reloaded: An improved model of biogeochemical cycling over Phanerozoic time. Earth-Science Reviews 178, 1-28.
Liu, A.-Q., Tang, D.-J., Shi, X.-Y., Zhou, L.-M., Zhou, X.-Q., Shang, M.-H., Li, Y., Song, H.-Y., 2019. Growth mechanisms and environmental implications of carbonate concretions from the~ 1.4 Ga Xiamaling Formation, North China. Journal of Palaeogeography 8(1), 20.
Londry, K.L., Dawson, K.G., Grover, H.D., Summons, R.E., Bradley, A.S., 2008. Stable carbon isotope fractionation between substrates and products of Methanosarcina barkeri. Organic Geochemistry 39(5), 608-621.

Lowenstein, T.K., Hardie, L.A., Timofeeff, M.N., Demicco, R.V., 2003. Secular variation in seawater chemistry and the origin of calcium chloride basinal brines. Geology 31(10), 857-860.
Loyd, S., Berelson, W., 2016. The modern record of "concretionary" carbonate: Reassessing a discrepancy between modern sediments and the geologic record. Chemical Geology 420, 77-87.
Loyd, S.J., Corsetti, F.A., Eiler, J.M., Tripati, A.K., 2012. Determining the diagenetic conditions of concretion formation: assessing temperatures and pore waters using clumped isotopes. Journal of Sedimentary Research 82(12), 1006-1016.
Loyd, S.J., Smirnoff, M.N., 2022. Progressive formation of authigenic carbonate with depth in siliciclastic marine sediments including substantial formation in sediments experiencing methanogenesis. Chemical Geology 594, 120775.
Luo, G., Kump, L.R., Wang, Y., Tong, J., Arthur, M.A., Yang, H., Huang, J., Yin, H., Xie, S., 2010. Isotopic evidence for an anomalously low oceanic sulfate concentration following end-Permian mass extinction. Earth and Planetary Science Letters 300(1-2), 101-111.
Lyons, T., Reinhard, C., Scott, C., 2009. Redox redux. Geobiology 7(5), 489-494.
Lyons, T.W., Reinhard, C.T., Planavsky, N.J., 2014. The rise of oxygen in Earth's early ocean and atmosphere. Nature 506(7488), 307-315.
Maheshwari, A., Sial, A.N., Gaucher, C., Bossi, J., Bekker, A., Ferreira, V.P., Romano, A.W., 2010. Global nature of the Paleoproterozoic Lomagundi carbon isotope excursion: A review of occurrences in Brazil, India, and Uruguay. Precambrian Research 182(4), 274-299.
Martill, D., 1988. Preservation of fish in the Cretaceous Santana Formation of Brazil. Palaeontology 31(1), 1-18.
McCarty, P.L., 1964. The methane fermentation. Principles and applications in aquatic microbiology, 314-343.
Meister, P., Liu, B., Ferdelman, T.G., Jørgensen, B.B., Khalili, A., 2013. Control of sulphate and methane distributions in marine sediments by organic matter reactivity. Geochimica et Cosmochimica Acta 104, 183-193.
Meister, P., Liu, B., Khalili, A., Böttcher, M.E., Jørgensen, B.B., 2019. Factors controlling the carbon isotope composition of dissolved inorganic carbon and methane in marine porewater: An evaluation by reaction-transport modelling. Journal of Marine Systems 200, 103227.
Meister, P., Reyes, C., 2019. The carbon-isotope record of the sub-seafloor biosphere. Geosciences 9(12), 507.
Melezhik, V.A., Fallick, A.E., 1996. A widespread positive δ13Ccarb anomaly at around 2.33–2.06 Ga on the Fennoscandian Shield: a paradox? Terra Nova 8(2), 141-157.
Mozley, P.S., Burns, S.J., 1993. Oxygen and carbon isotopic composition of marine carbonate concretions: an overview. Journal of Sedimentary Research 63(1), 73-83.
Och, L.M., Shields-Zhou, G.A., 2012. The Neoproterozoic oxygenation event: environmental perturbations and biogeochemical cycling. Earth-Science Reviews 110(1-4), 26-57.
Ohkouchi, N., Kawamura, K., Kajiwara, Y., Wada, E., Okada, M., Kanamatsu, T., Taira, A., 1999. Sulfur isotope records around Livello Bonarelli (northern Apennines, Italy) black shale at the Cenomanian-Turonian boundary. Geology 27(6), 535-538.

Ohmoto, H., Rye, R.O., 1979. Isotopes of sulfur and carbon. Geochemistry of hydrothermal ore deposits, 509-567.
Orphan, V.J., Ussler, W., Naehr, T.H., House, C.H., Hinrichs, K.U., Paull, C.K., 2004. Geological, geochemical, and microbiological heterogeneity of the seafloor around methane vents in the Eel River Basin, offshore California. Chemical Geology 205(3-4), 265-289.
Partin, C., Bekker, A., Planavsky, N., Scott, C., Gill, B., Li, C., Podkovyrov, V., Maslov, A., Konhauser, K., Lalonde, S., 2013. Large-scale fluctuations in Precambrian atmospheric and oceanic oxygen levels from the record of U in shales. Earth and Planetary Science Letters 369, 284-293.
Paull, C., Lorenson, T., Borowski, W., Ussler Iii, W., Olsen, K., Rodriguez, N., 2000. Isotopic composition of CH4, CO2 species, and sedimentary organic matter within samples from the Blake Ridge: Gas source implications. Proceedings of the Ocean Drilling Program, Initial Reports 164, 67-78.
Pisciotto, K.A., Mahoney, J.J., 1981. Authigenic dolomite in Monterey Formation, California, and related rocks from offshore California and Baja California. AAPG Bulletin 65(5), 972-973.
Planavsky, N.J., Bekker, A., Hofmann, A., Owens, J.D., Lyons, T.W., 2012. Sulfur record of rising and falling marine oxygen and sulfate levels during the Lomagundi event. Proc Natl Acad Sci U S A 109(45), 18300-18305. doi.org/10.1073/pnas.1120387109.
Planavsky, N.J., Fakhraee, M., Bolton, E.W., Reinhard, C.T., Isson, T.T., Zhang, S., Mills, B.J., 2022. On carbon burial and net primary production through Earth's history. American Journal of Science 322(3), 413-460.
Planavsky, N.J., McGoldrick, P., Scott, C.T., Li, C., Reinhard, C.T., Kelly, A.E., Chu, X., Bekker, A., Love, G.D., Lyons, T.W., 2011. Widespread iron-rich conditions in the mid-Proterozoic ocean. Nature 477(7365), 448-451.
Pohlman, J.W., Ruppel, C., Hutchinson, D.R., Downer, R., Coffin, R.B., 2008. Assessing sulfate reduction and methane cycling in a high salinity pore water system in the northern Gulf of Mexico. Marine and Petroleum Geology 25(9), 942-951.
Pope, M.C., Grotzinger, J.P., 2003. Paleoproterozoic Stark Formation, Athapuscow basin, northwest Canada: Record of cratonic-scale salinity crisis. Journal of Sedimentary Research 73(2), 280-295.
Poulton, S., Raiswell, R., 2002. The low-temperature geochemical cycle of iron: from continental fluxes to marine sediment deposition. American journal of science 302(9), 774-805.
Poulton, S.W., Fralick, P.W., Canfield, D.E., 2010. Spatial variability in oceanic redox structure 1.8 billion years ago. Nature Geoscience 3(7), 486-490.
Prave, A., Kirsimäe, K., Lepland, A., Fallick, A., Kreitsmann, T., Deines, Y.E., Romashkin, A., Rychanchik, D., Medvedev, P., Moussavou, M., 2022. The grandest of them all: the Lomagundi–Jatuli Event and Earth's oxygenation. Journal of the Geological Society 179(1).
Price, N., Calvert, S., 1973. The geochemistry of iodine in oxidised and reduced recent marine sediments. Geochimica et Cosmochimica Acta 37(9), 2149-2158.
Raiswell, R., 1971. The growth of Cambrian and Liassic concretions. Sedimentology 17(3‐4), 147-171.

Raiswell, R., Berner, R.A., 1986. Pyrite and organic matter in Phanerozoic normal marine shales. Geochimica et Cosmochimica Acta 50(9), 1967-1976.
Raiswell, R., Canfield, D.E., 1998. Sources of iron for pyrite formation in marine sediments. American Journal of Science 298(3), 219-245.
Ronov, A., Khain, V., Balukhovsky, A., Seslavinsky, K., 1980. Quantitative analysis of Phanerozoic sedimentation. Sedimentary Geology 25(4), 311-325.
Sackett, W.M., Poag, C.W., Eadie, B.J., 1974. Kerogen recycling in the Ross sea, Antarctica. Science 185(4156), 1045-1047.
Sahoo, S.K., Planavsky, N.J., Kendall, B., Wang, X., Shi, X., Scott, C., Anbar, A.D., Lyons, T.W., Jiang, G., 2012. Ocean oxygenation in the wake of the Marinoan glaciation. Nature 489(7417), 546-549.
Salop, L., 1982. Geologic Development of the Earth in Precambrian. Nedra, Leningrad, 343.
Savrda, C.E., Bottjer, D.J., 1988. Limestone concretion growth documented by trace-fossil relations. Geology 16(10), 908-911.
Schidlowski, M., Eichmann, R., Junge, C.E., 1975. Precambrian sedimentary carbonates: carbon and oxygen isotope geochemistry and implications for the terrestrial oxygen budget. Precambrian Research 2(1), 1-69.
Schidlowski, M., Eichmann, R., Junge, C.E., 1976. Carbon isotope geochemistry of the Precambrian Lomagundi carbonate province, Rhodesia. Geochimica et Cosmochimica Acta 40(4), 449-455.
Schlünz, B., Schneider, R.R., 2000. Transport of terrestrial organic carbon to the oceans by rivers: re-estimating flux-and burial rates. International Journal of Earth Sciences 88(4), 599-606.
Schrag, D.P., Higgins, J.A., Macdonald, F.A., Johnston, D.T., 2013. Authigenic carbonate and the history of the global carbon cycle. science 339(6119), 540-543.
Schröder, S., Bekker, A., Beukes, N., Strauss, H., Van Niekerk, H., 2008. Rise in seawater sulphate concentration associated with the Paleoproterozoic positive carbon isotope excursion: evidence from sulphate evaporites in the∼ 2.2–2.1 Gyr shallow‐marine Lucknow Formation, South Africa. Terra Nova 20(2), 108-117.
Scotchman, I., 1991. The geochemistry of concretions from the Kimmeridge Clay Formation of southern and eastern England. Sedimentology 38(1), 79-106.
Scott, C., Lyons, T., Bekker, A., Shen, Y.-a., Poulton, S., Chu, X.-l., Anbar, A., 2008. Tracing the stepwise oxygenation of the Proterozoic ocean. Nature 452(7186), 456-459.
Seewald, J.S., 2003. Organic–inorganic interactions in petroleum-producing sedimentary basins. Nature 426(6964), 327-333.
Shi, W., Mills, B.J., Li, C., Poulton, S.W., Krause, A.J., He, T., Zhou, Y., Cheng, M., Shields, G.A., 2022. Decoupled oxygenation of the Ediacaran ocean and atmosphere during the rise of early animals. Earth and Planetary Science Letters 591, 117619.
Sivan, O., Schrag, D., Murray, R., 2007. Rates of methanogenesis and methanotrophy in deep‐sea sediments. Geobiology 5(2), 141-151.
Skei, J., 1983. Permanently Anoxic Marine Basins: Exchange of Substances across Boundaries. Ecological Bulletins, 419-429.
Song, H., Tong, J., Algeo, T.J., Song, H., Qiu, H., Zhu, Y., Tian, L., Bates, S., Lyons, T.W., Luo, G., 2014. Early Triassic seawater sulfate drawdown. Geochimica et Cosmochimica Acta 128, 95-113.

Sperling, E.A., Stockey, R.G., 2018. The temporal and environmental context of early animal evolution: Considering all the ingredients of an "explosion". Integrative and Comparative Biology 58(4), 605-622.
Sperling, E.A., Wolock, C.J., Morgan, A.S., Gill, B.C., Kunzmann, M., Halverson, G.P., Macdonald, F.A., Knoll, A.H., Johnston, D.T., 2015. Statistical analysis of iron geochemical data suggests limited late Proterozoic oxygenation. Nature 523(7561), 451-454.
Sunagawa, I., 1994. Nucleation, growth and dissolution of crystals during sedimentogenesis and diagenesis, Developments in Sedimentology. Elsevier, pp. 19-47.
Tosca, N.J., Johnston, D.T., Mushegian, A., Rothman, D.H., Summons, R.E., Knoll, A.H., 2010. Clay mineralogy, organic carbon burial, and redox evolution in Proterozoic oceans. Geochimica et Cosmochimica Acta 74(5), 1579-1592.
Veizer, J., Ala, D., Azmy, K., Bruckschen, P., Buhl, D., Bruhn, F., Carden, G.A., Diener, A., Ebneth, S., Godderis, Y., 1999. 87Sr/86Sr, δ13C and δ18O evolution of Phanerozoic seawater. Chemical geology 161(1), 59-88.
Whiticar, M.J., 1999. Carbon and hydrogen isotope systematics of bacterial formation and oxidation of methane. Chemical Geology 161(1), 291-314.
Whiticar, M.J., Faber, E., Schoell, M., 1986. Biogenic methane formation in marine and freshwater environments: CO2 reduction vs. acetate fermentation—isotope evidence. Geochimica et Cosmochimica Acta 50(5), 693-709.
Wortmann, U.G., Chernyavsky, B.M., 2007. Effect of evaporite deposition on Early Cretaceous carbon and sulphur cycling. Nature 446(7136), 654-656.
Yoshida, H., Ujihara, A., Minami, M., Asahara, Y., Katsuta, N., Yamamoto, K., Sirono, S.-i., Maruyama, I., Nishimoto, S., Metcalfe, R., 2015. Early post-mortem formation of carbonate concretions around tusk-shells over week-month timescales. Scientific reports 5, 1-7.
Yoshinaga, M.Y., Holler, T., Goldhammer, T., Wegener, G., Pohlman, J.W., Brunner, B., Kuypers, M.M., Hinrichs, K.-U., Elvert, M., 2014. Carbon isotope equilibration during sulphate-limited anaerobic oxidation of methane. Nature Geoscience 7(3), 190-194.
Zeebe, R.E., 2007. Modeling CO2 chemistry, δ13C, and oxidation of organic carbon and methane in sediment porewater: Implications for paleo-proxies in benthic foraminifera. Geochimica et Cosmochimica Acta 71(13), 3238-3256.

Figure Captions

Figure 1: Abundance of concretion-bearing units through time. a) Entire distribution in 100-myr age bins. b) 3000 to 1000 Ma, notice concretion-rich interval following the Archean Proterozoic boundary. c) 950 Ma to present in 25-myr age bins. Panels b and c indicate $\delta^{13}C$ coverage.

Figure 2: Concretion a) mineralogy and b) host lithology. Note scale compression for 1000 Ma and older bins.

Figure 3: $\Delta^{13}C_{con\text{-}sw}$ variability a) since 3000 Ma and b) since the latest Proterozoic. Shaded envelope encompasses expected seawater values and dashed line indicates minimum values for organic matter oxidation (–25‰). Normal and septarian concretions and associated crystal habits indicated by symbols.

Figure 4: $\Delta^{13}C_{con\text{-}sw}$ a) mean, b) minimum (min.), c) maximum (max.) and d) ranges for different age intervals. Precambrian data provided with (All) and without (- Lomag.) Lomagundi-aged samples. Notice decrease in minimum and increase in maximum and ranges through time.

Figure 5: Marine organic carbon burial and $\Delta^{13}C_{con\text{-}sw}$. a) Temporal variability since 3000 Ma and b) 600 Ma. Organic carbon burial data after model reconstructions of Planavsky et al. (2022) and Krissansen‐Totton et al. (2021). Organic carbon burial after low

erosion rate, low overbank oxidation results of Planavsky et al. (2022) (Fig. 14a from that work), other result show similar trends but with potentially different absolute values.

Figure 6: Iron speciation data and $\Delta^{13}C_{con\text{-}sw}$ (gray symbols). a) all iron data, b) data from samples with FeHR/FeT $\leq$ 0.38 wt.%. Notice lack of increase in iron contents through time and in particular across the Proterozoic-Paleozoic transition. Correlation plots and iron data references provided in Supplementary Material.

Figure 7: Marine sulfate concentrations and $\Delta^{13}C_{con\text{-}sw}$ (gray symbols). a) Temporal variability since 3000 Ma and b) 600 Ma. Sulfate concentrations from Planavsky et al. (2012), MSR-method of Algeo et al. (2015), Fakhraee et al. (2018), Fakhraee et al. (2019), Shi et al. (2022), Habicht et al. (2002), Berner (2004), Halevy et al. (2012), Blättler et al. (2018), Blättler et al. (2020), LaFlamme et al. (2021) and Krause et al. (2022).

Figure 8: Porewater model results demonstrating potential controls on $\delta^{13}C_{DIC}$ and comparison to concretion record. Solid and dashed gray lines in a-c represent marine DIC and organic matter $\delta^{13}C$, respectively. a) impact of marine sulfate content. Note that as sulfate concentrations increase, both $\delta^{13}C_{DIC}$ minimum and maximum values decrease. b) impact of external methane flux under modern marine sulfate concentrations. External methane $\delta^{13}C$ values are assigned the value achieved at the base of the modeled domain, deviations from this value impact the minimum $\delta^{13}C_{DIC}$. Note that as external methane input increases, $\delta^{13}C_{DIC}$ minimum values decrease and yield compositions below the

organic matter $\delta^{13}C$ value. c) impact of marine sulfate content under variable external methane flux (ext. CH_4 flux). Increased sulfate contents yield decreased $\delta^{13}C_{DIC}$ minimum and maximum values similar to overall trends observed in a. Note that $\delta^{13}C_{DIC}$ depletions produce minimum values that drop well below the organic matter $\delta^{13}C$ value under high sulfate conditions. Maximum data trends overlap. In a-c, $\alpha_{methane\text{-}DIC} = 0.94$ and the isotopic difference between methane and DIC was maintained at ~75‰. d) comparison between marine sulfate concentrations and minimum $\Delta^{13}C_{con\text{-}sw}$ for the age groupings discussed in the text. Blue bands represent ranges from Fakhraee et al., 2018, 2019, all other data are sulfate concentration averages. Notice decrease in minimum isotope compositions with increasing sulfate content, similar to minimum model data in c. Linear regressions and correlation strengths also provided.

Figure 9: Modeled variability in $\delta^{13}C_{DIC}$ as a function of marine DIC content across a range of marine sulfate concentrations. Increasing marine DIC yields higher $\delta^{13}C_{DIC}$ minima except under the 0 mM sulfate condition. This increase is more pronounced at lower marine sulfate concentrations. The $\delta^{13}C_{DIC}$ maxima are relatively invariant.

Figure 10: Comparison between organic carbon burial and minimum $\Delta^{13}C_{con\text{-}sw}$ for the age groupings discussed in the text.

Figure 11: Impacts of organic carbon burial on isotope compositions. a) Comparison between organic carbon burial and maximum $\Delta^{13}C_{con\text{-}sw}$ for the age groupings discussed in the text. b) Modeled variability in $\delta^{13}C_{DIC}$ as a function of total organic carbon (TOC)

1304 deposited at the sediment water interface. As TOC contents increase $\delta^{13}C_{DIC}$ maximum

1305 values increase, but do not exceed ~ +15‰.

1306

1307
1308
1309

Figure Captions

Figure 1: Abundance of concretion-bearing units through time. a) Entire distribution in 100-myr age bins. b) 3000 to 1000 Ma, notice concretion-rich interval following the Archean Proterozoic boundary. c) 950 Ma to present in 25-myr age bins. Panels b and c indicate $\delta^{13}C$ coverage.

Figure 2: Concretion a) mineralogy and b) host lithology. Note scale compression for 1000 Ma and older bins.

Figure 3: $\Delta^{13}C_{con\text{-}sw}$ variability a) since 3000 Ma and b) since the latest Proterozoic. Shaded envelope encompasses expected seawater values and dashed line indicates minimum values for organic matter oxidation (–25‰). Normal and septarian concretions and associated crystal habits indicated by symbols.

Figure 4: $\Delta^{13}C_{con\text{-}sw}$ a) mean, b) minimum (min.), c) maximum (max.) and d) ranges for different age intervals. Precambrian data provided with (All) and without (- Lomag.) Lomagundi-aged samples. Notice decrease in minimum and increase in maximum and ranges through time.

Figure 5: Marine organic carbon burial and $\Delta^{13}C_{con\text{-}sw}$. a) Temporal variability since 3000 Ma and b) 600 Ma. Organic carbon burial data after model reconstructions of Planavsky et al. (2022) and Krissansen‐Totton et al. (2021). Organic carbon burial after low

erosion rate, low overbank oxidation results of Planavsky et al. (2022) (Fig. 14a from that work), other result show similar trends but with potentially different absolute values.

Figure 6: Iron speciation data and $\Delta^{13}C_{con\text{-}sw}$ (gray symbols). a) all iron data, b) data from samples with FeHR/FeT ≤ 0.38 wt.%. Notice lack of increase in iron contents through time and in particular across the Proterozoic-Paleozoic transition. Correlation plots and iron data references provided in Supplementary Material.

Figure 7: Marine sulfate concentrations and $\Delta^{13}C_{con\text{-}sw}$ (gray symbols). a) Temporal variability since 3000 Ma and b) 600 Ma. Sulfate concentrations from Planavsky et al. (2012), MSR-method of Algeo et al. (2015), Fakhraee et al. (2018), Fakhraee et al. (2019), Shi et al. (2022), Habicht et al. (2002), Berner (2004), Halevy et al. (2012), Blättler et al. (2018), Blättler et al. (2020), LaFlamme et al. (2021) and Krause et al. (2022).

Figure 8: Porewater model results demonstrating potential controls on $\delta^{13}C_{DIC}$ and comparison to concretion record. Solid and dashed gray lines in a-c represent marine DIC and organic matter $\delta^{13}C$, respectively. a) impact of marine sulfate content. Note that as sulfate concentrations increase, both $\delta^{13}C_{DIC}$ minimum and maximum values decrease. b) impact of external methane flux under modern marine sulfate concentrations. External methane $\delta^{13}C$ values are assigned the value achieved at the base of the modeled domain, deviations from this value impact the minimum $\delta^{13}C_{DIC}$. Note that as external methane input increases, $\delta^{13}C_{DIC}$ minimum values decrease and yield compositions below the

organic matter $\delta^{13}C$ value. c) impact of marine sulfate content under variable external methane flux (ext. CH_4 flux). Increased sulfate contents yield decreased $\delta^{13}C_{DIC}$ minimum and maximum values similar to overall trends observed in a. Note that $\delta^{13}C_{DIC}$ depletions produce minimum values that drop well below the organic matter $\delta^{13}C$ value under high sulfate conditions. Maximum data trends overlap. In a-c, $\alpha_{methane\text{-}DIC} = 0.94$ and the isotopic difference between methane and DIC was maintained at ~75‰. d) comparison between marine sulfate concentrations and minimum $\Delta^{13}C_{con\text{-}sw}$ for the age groupings discussed in the text. Blue bands represent ranges from Fakhraee et al., 2018, 2019, all other data are sulfate concentration averages. Notice decrease in minimum isotope compositions with increasing sulfate content, similar to minimum model data in c. Linear regressions and correlation strengths also provided.

Figure 9: Modeled variability in $\delta^{13}C_{DIC}$ as a function of marine DIC content across a range of marine sulfate concentrations. Increasing marine DIC yields higher $\delta^{13}C_{DIC}$ minima except under the 0 mM sulfate condition. This increase is more pronounced at lower marine sulfate concentrations. The $\delta^{13}C_{DIC}$ maxima are relatively invariant.

Figure 10: Comparison between organic carbon burial and minimum $\Delta^{13}C_{con\text{-}sw}$ for the age groupings discussed in the text.

Figure 11: Impacts of organic carbon burial on isotope compositions. a) Comparison between organic carbon burial and maximum $\Delta^{13}C_{con\text{-}sw}$ for the age groupings discussed in the text. b) Modeled variability in $\delta^{13}C_{DIC}$ as a function of total organic carbon (TOC)

deposited at the sediment water interface. As TOC contents increase $\delta^{13}C_{DIC}$ maximum values increase, but do not exceed ~ +15‰.

Figure 1

Click here to access/download:Figure:F1 Con dist.pdf

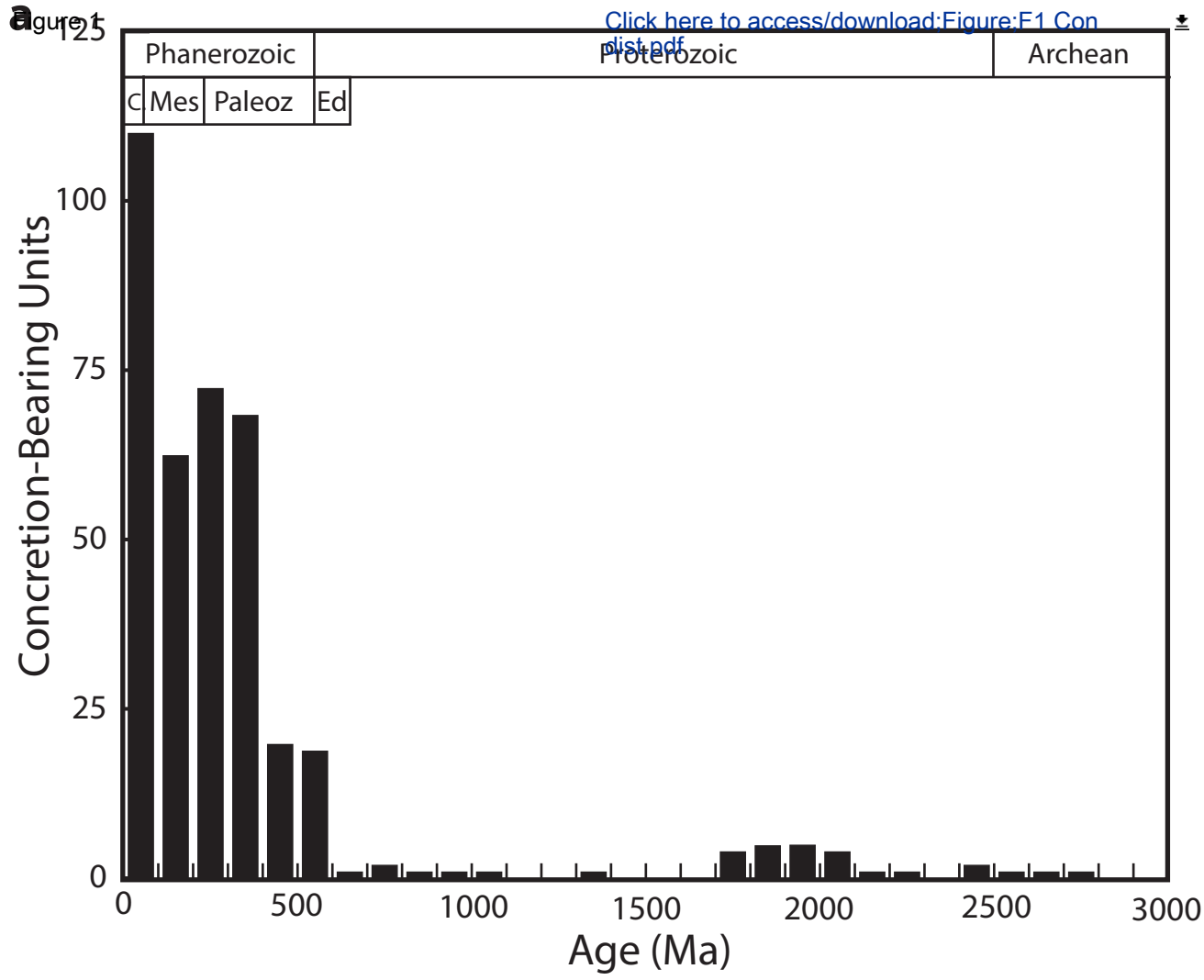

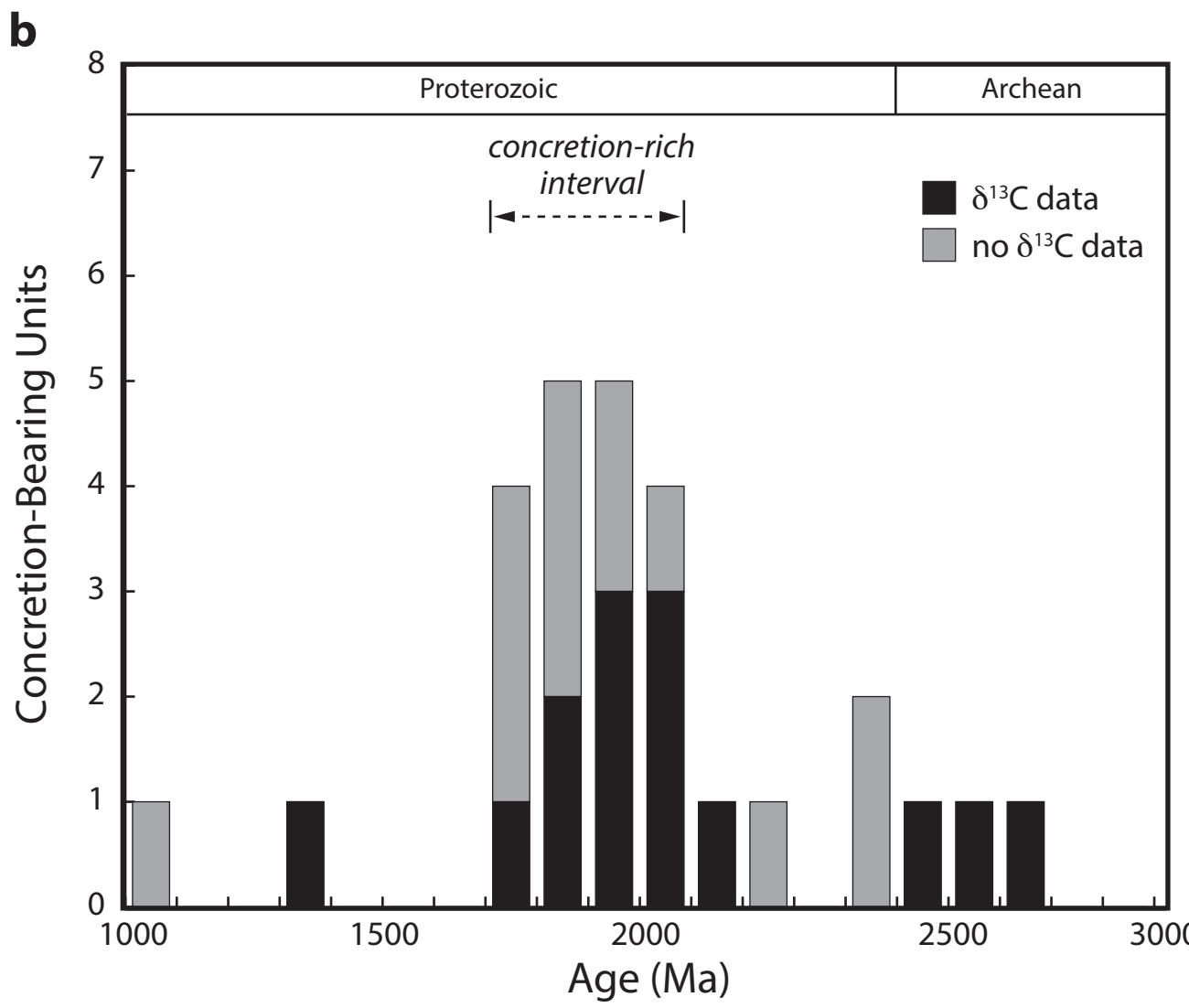

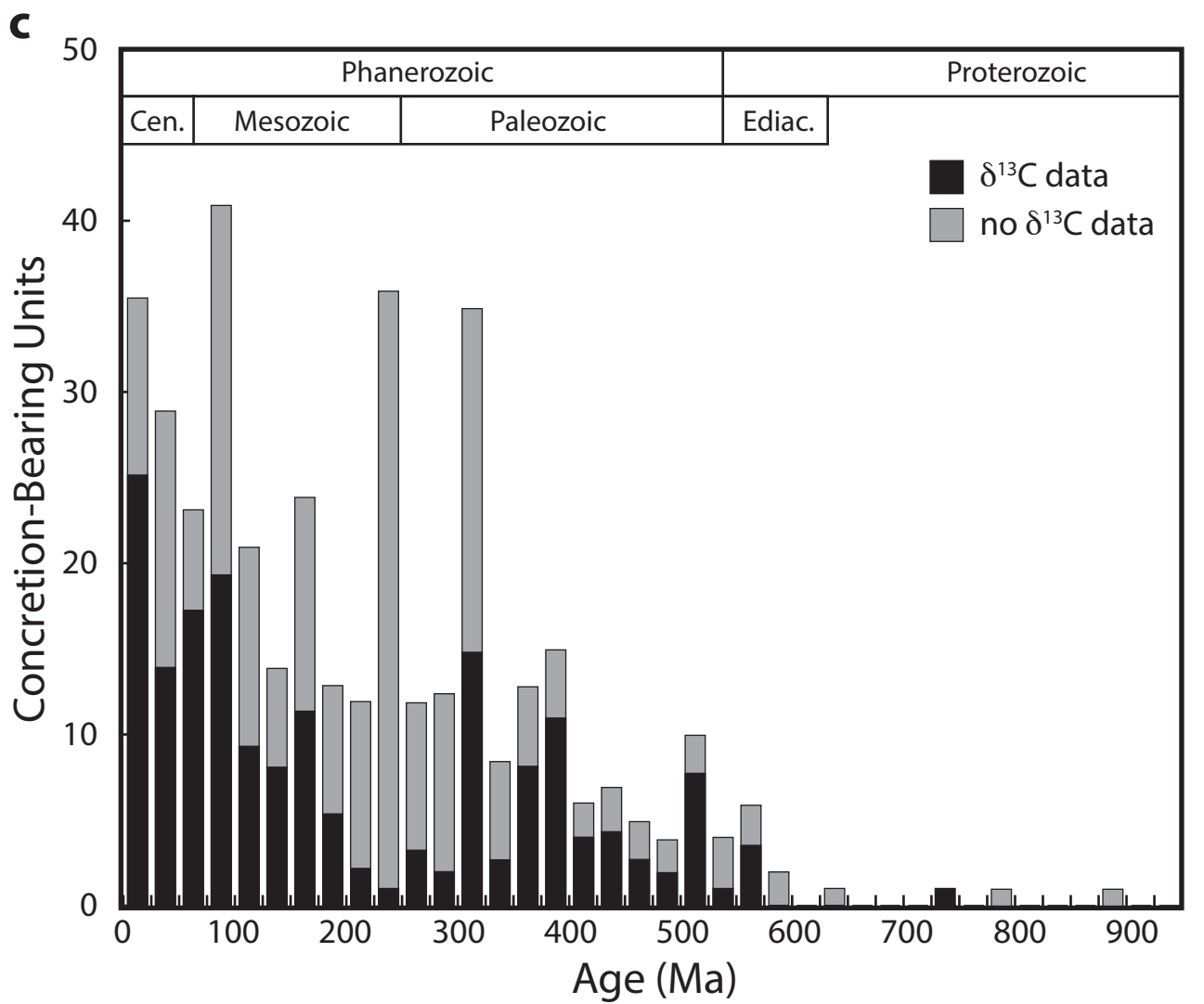

Figure 2

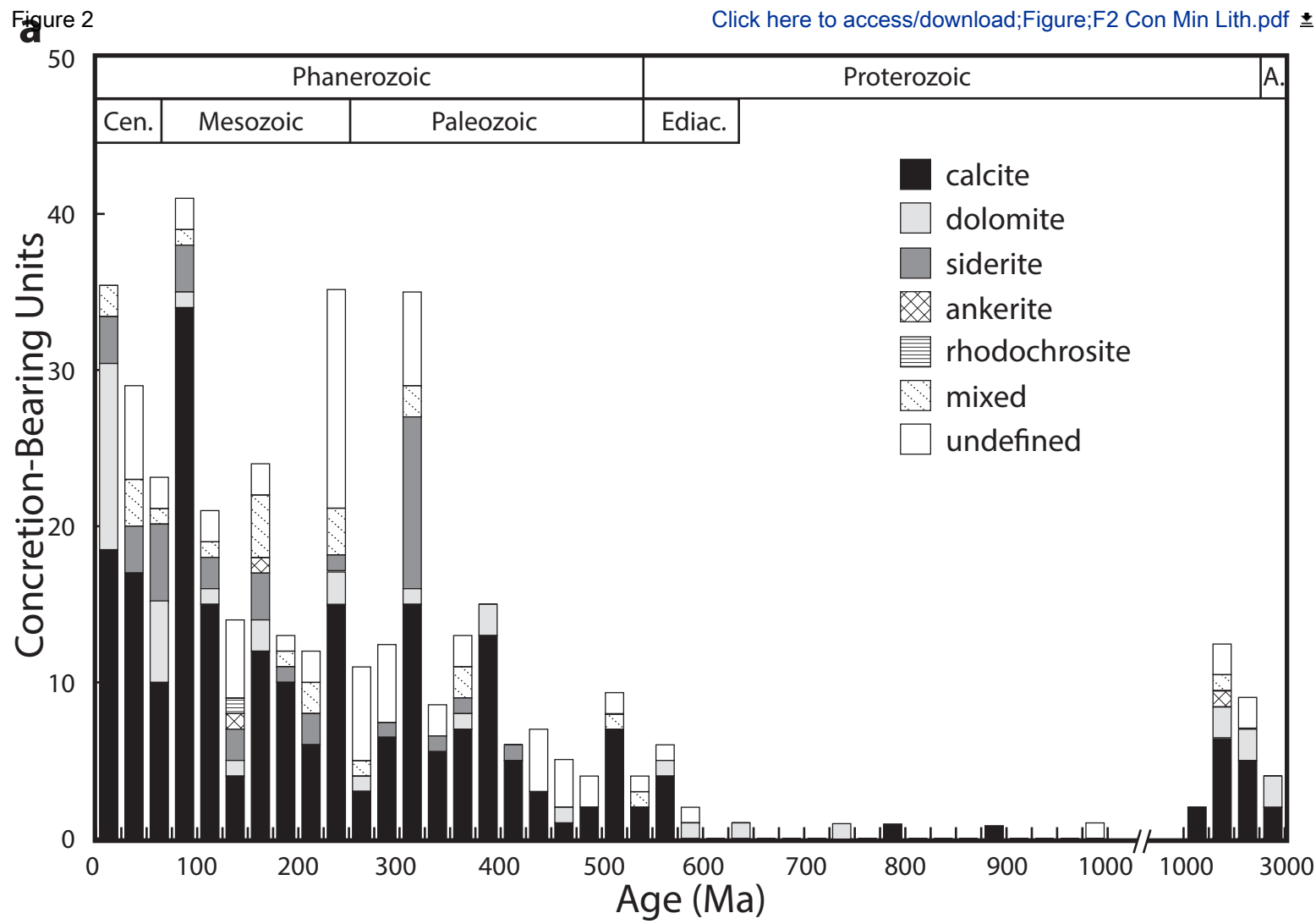

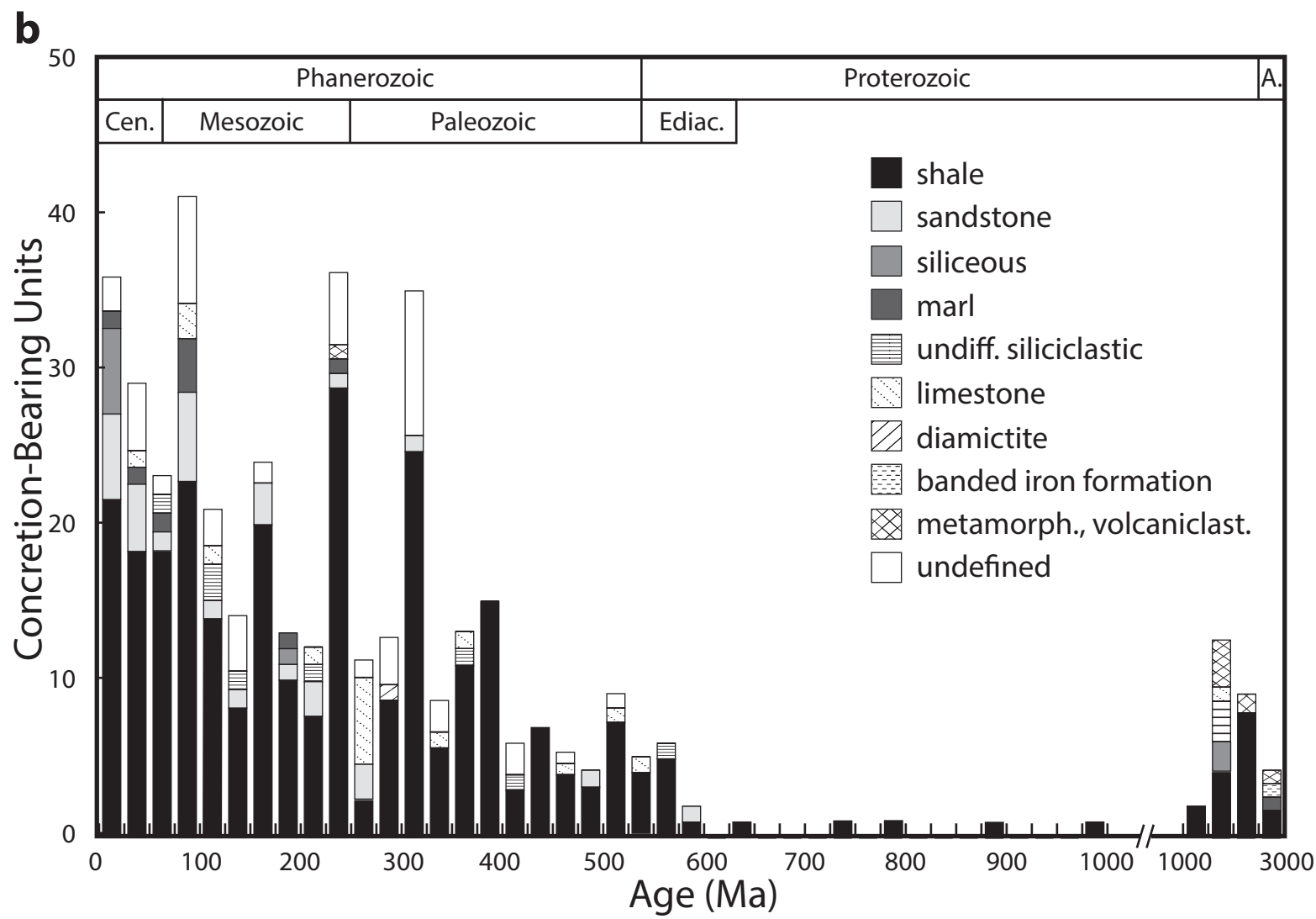

Figure 3

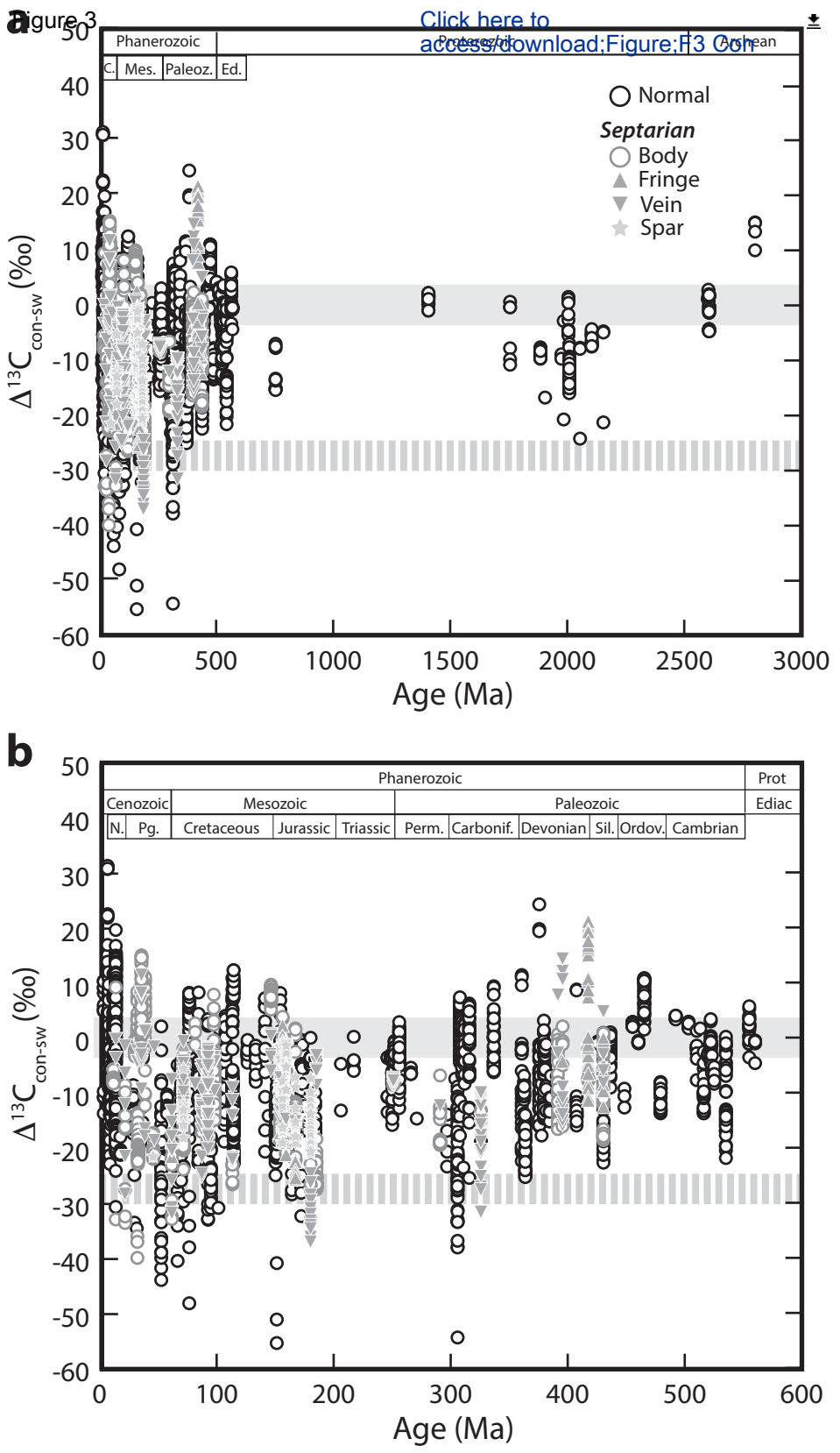

Figure 4

Click here to access/download:Figure:F4 Stats.pdf

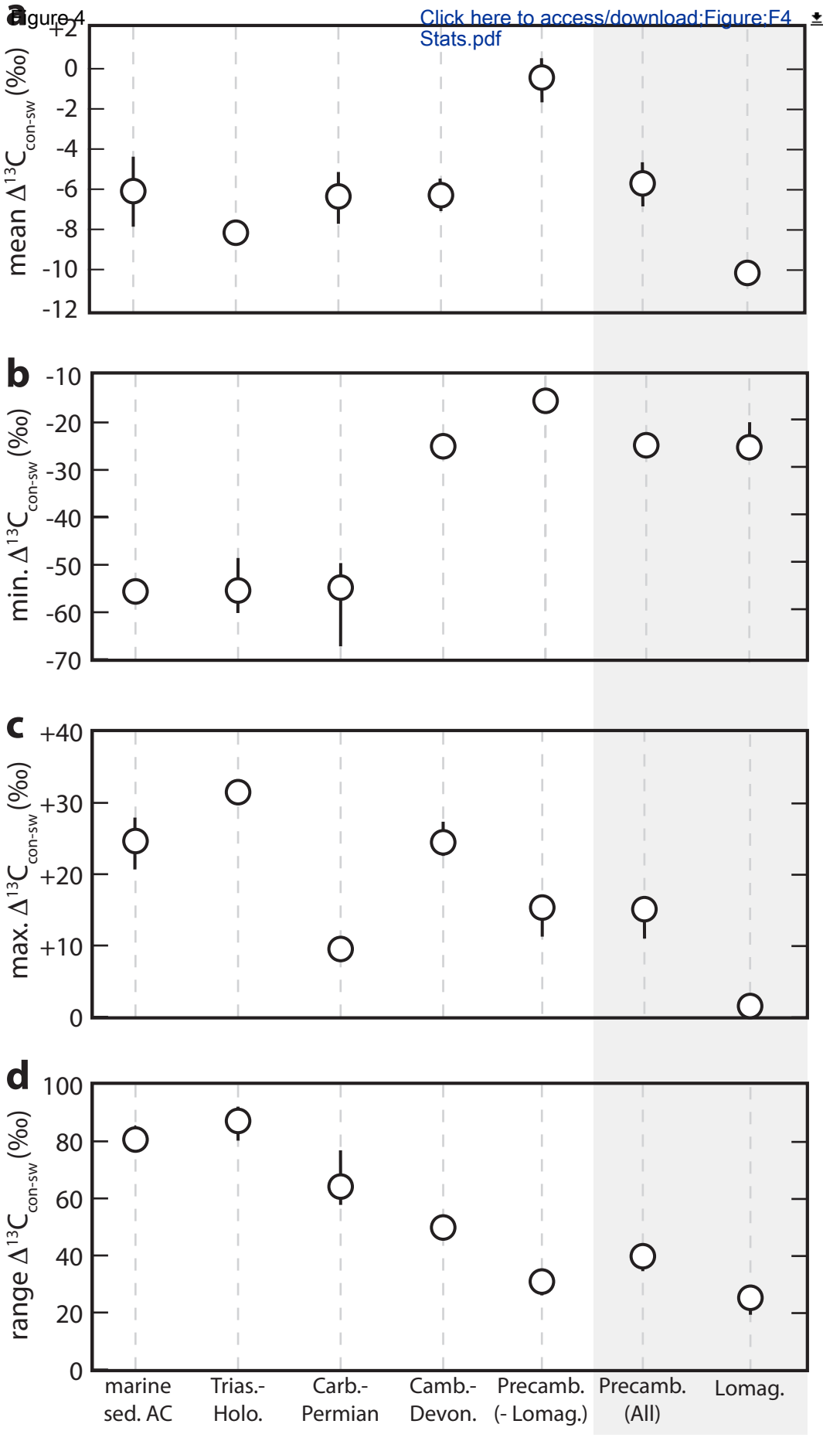

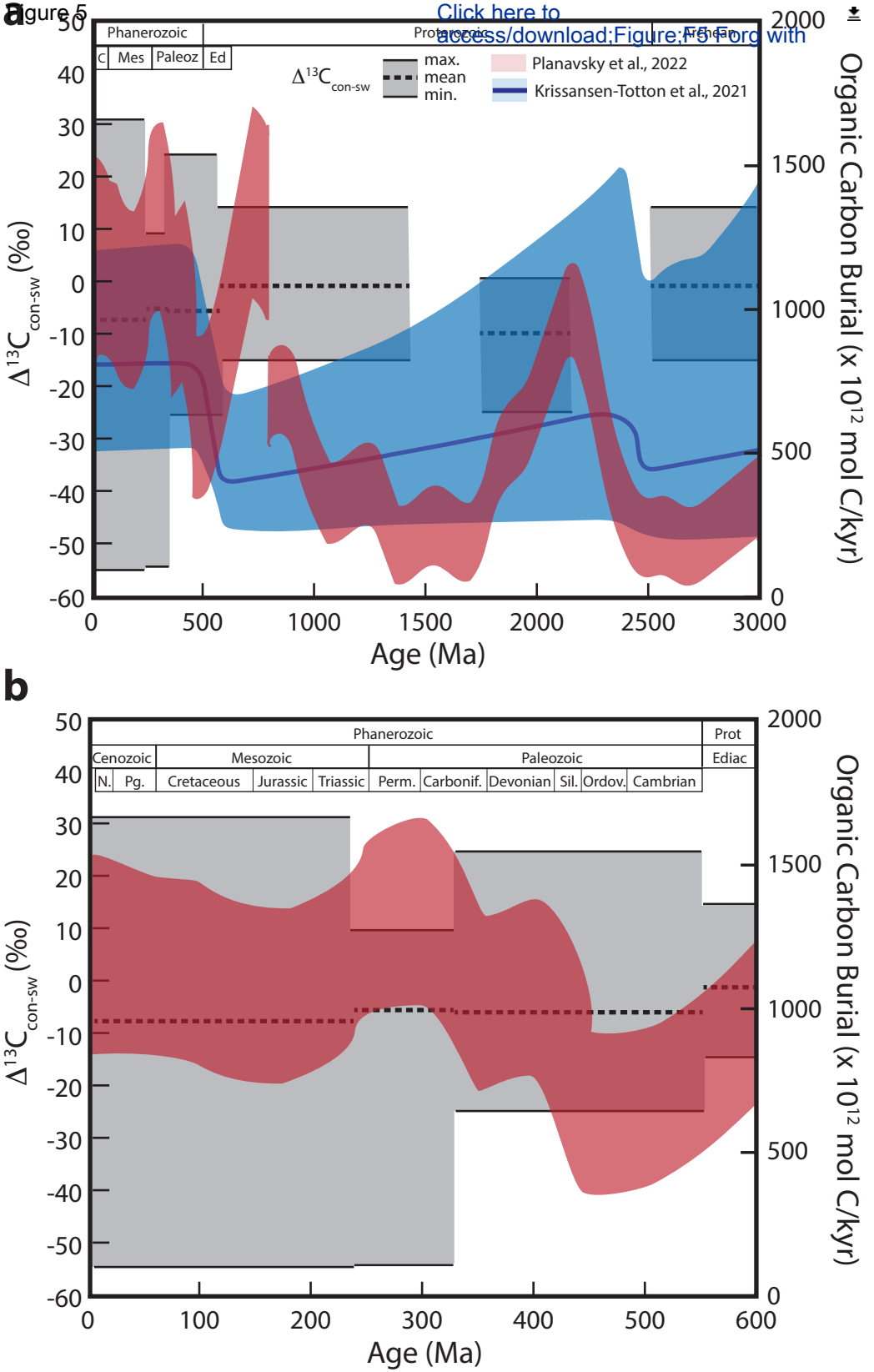

Figure 6

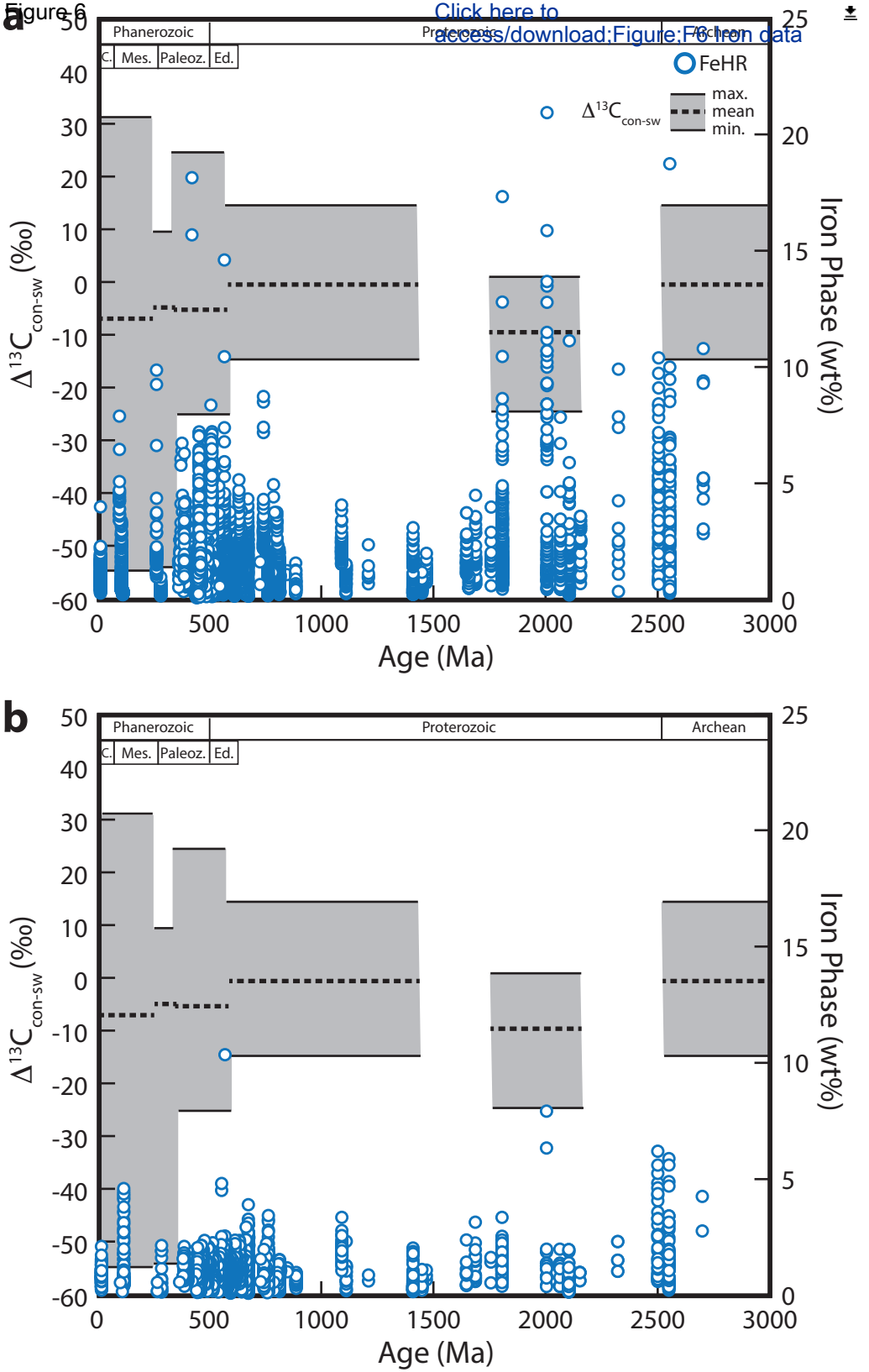

Figure 7

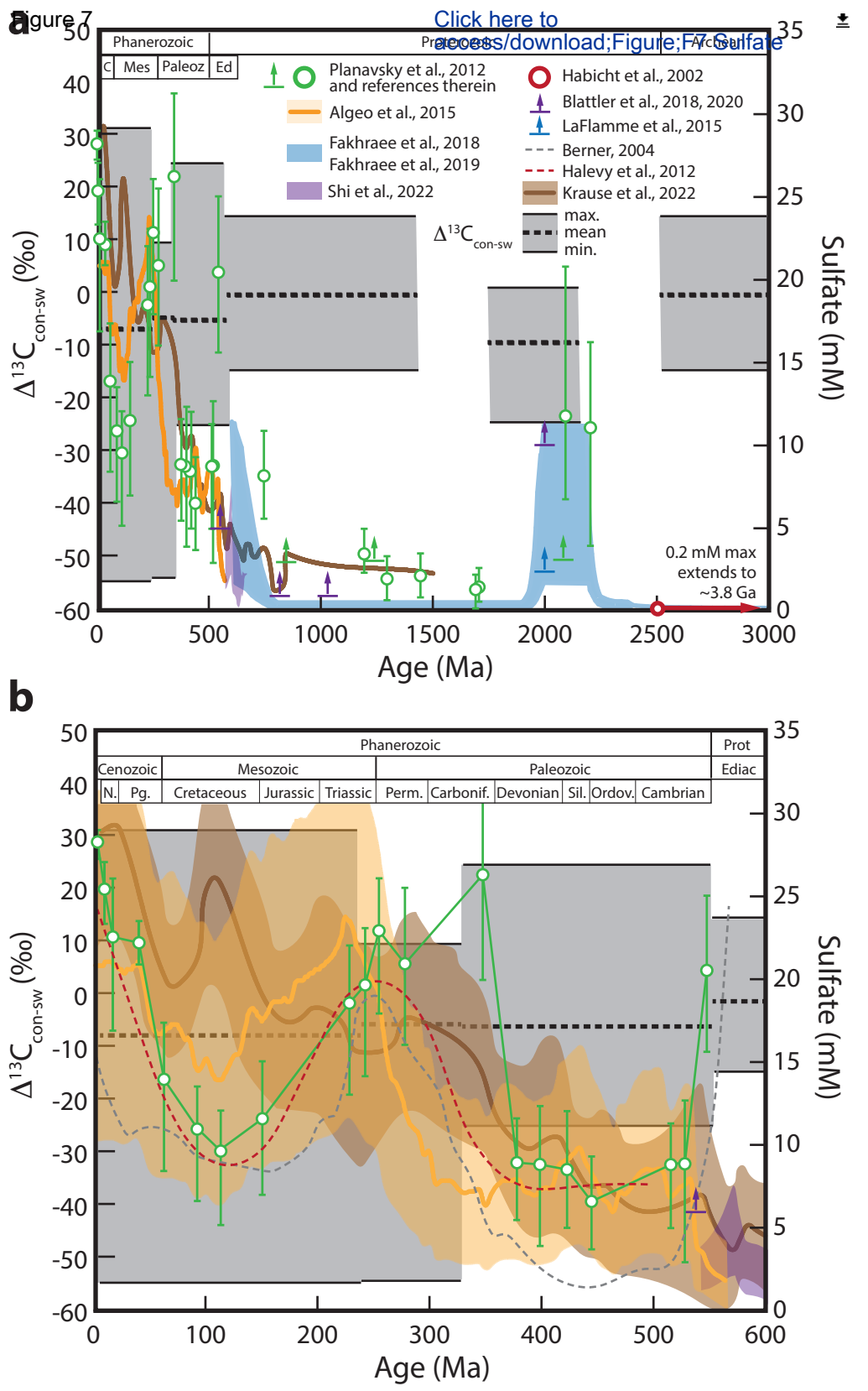

Figure 8

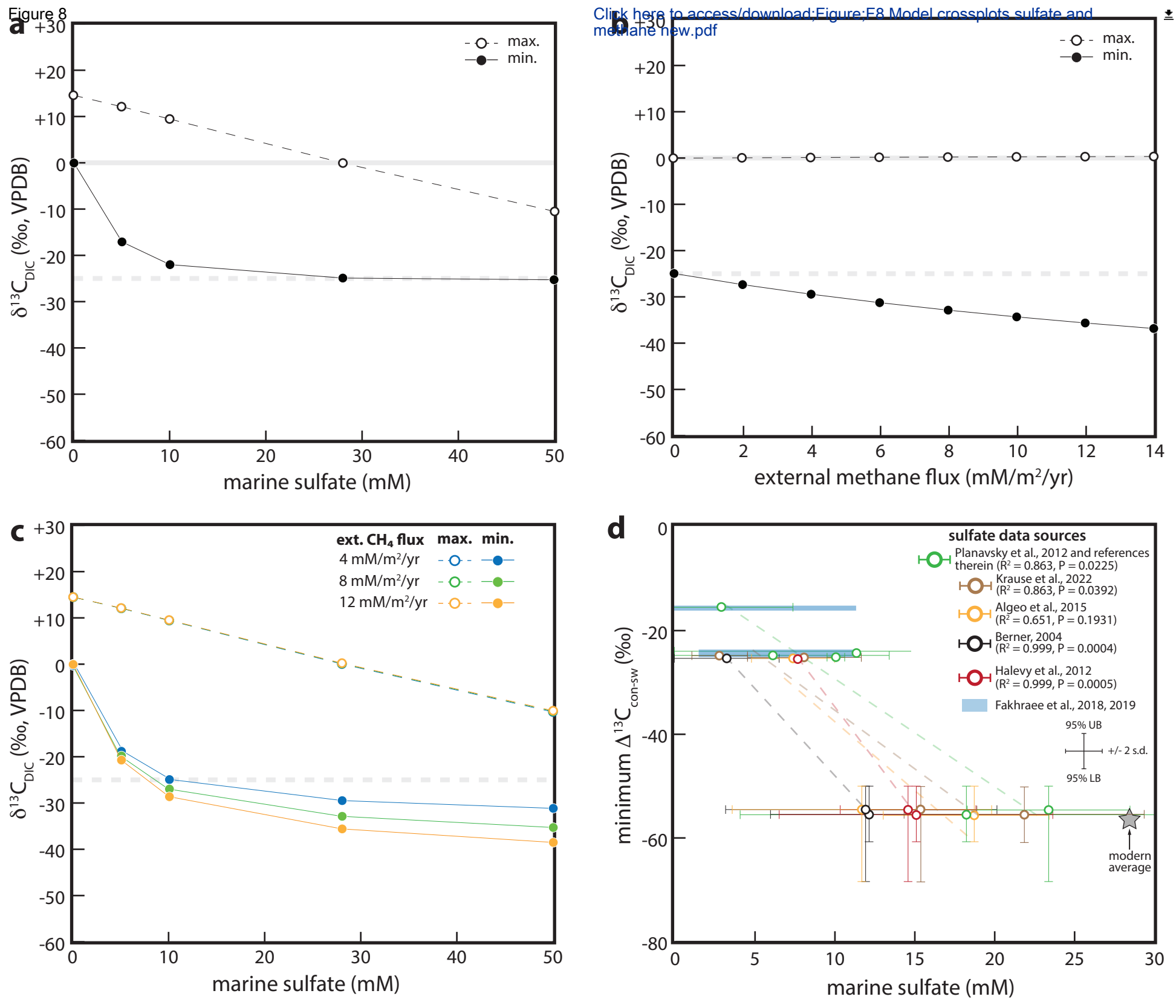

Figure 9

Click here to access/download;Figure;F9 Model

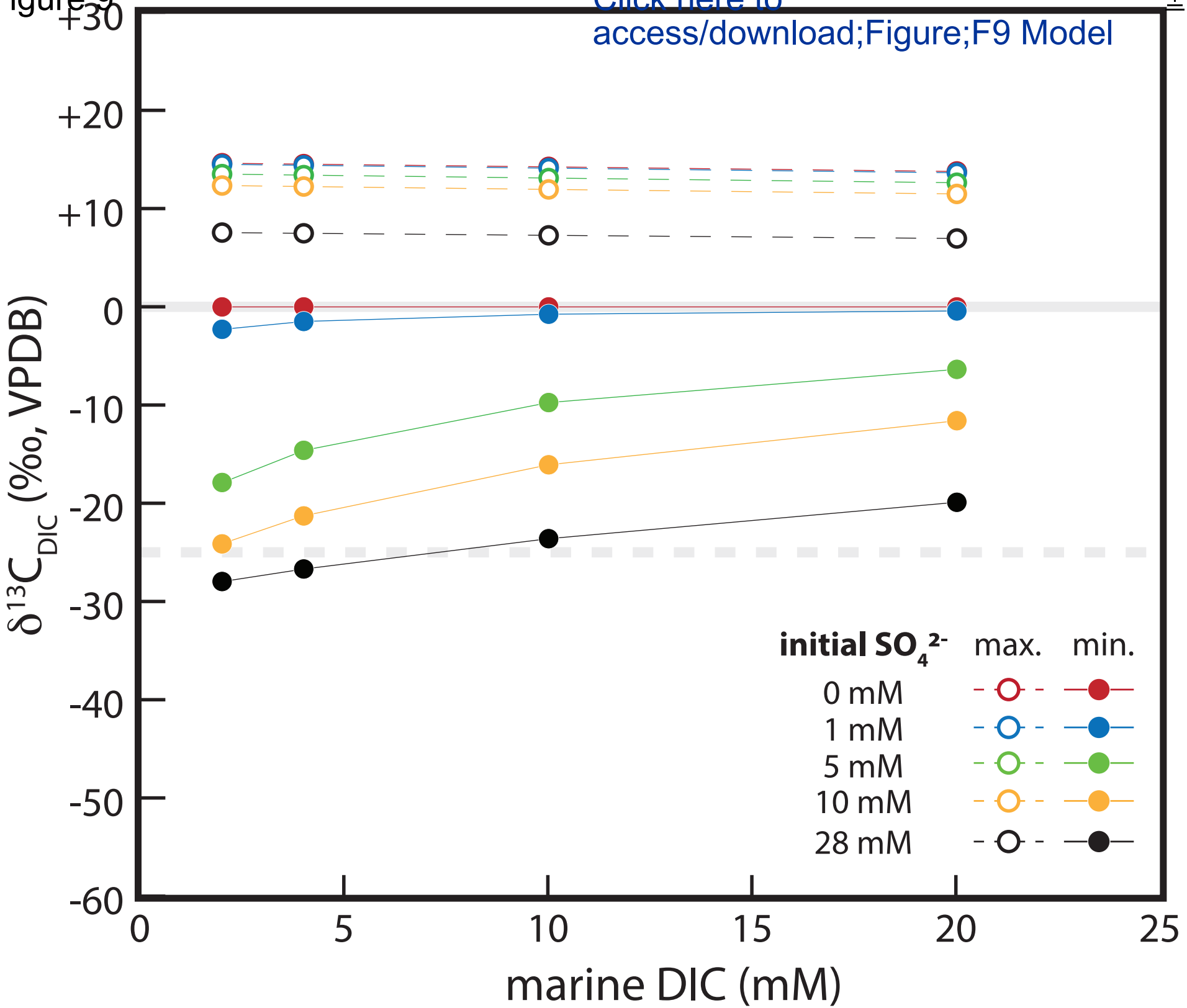

Figure 10

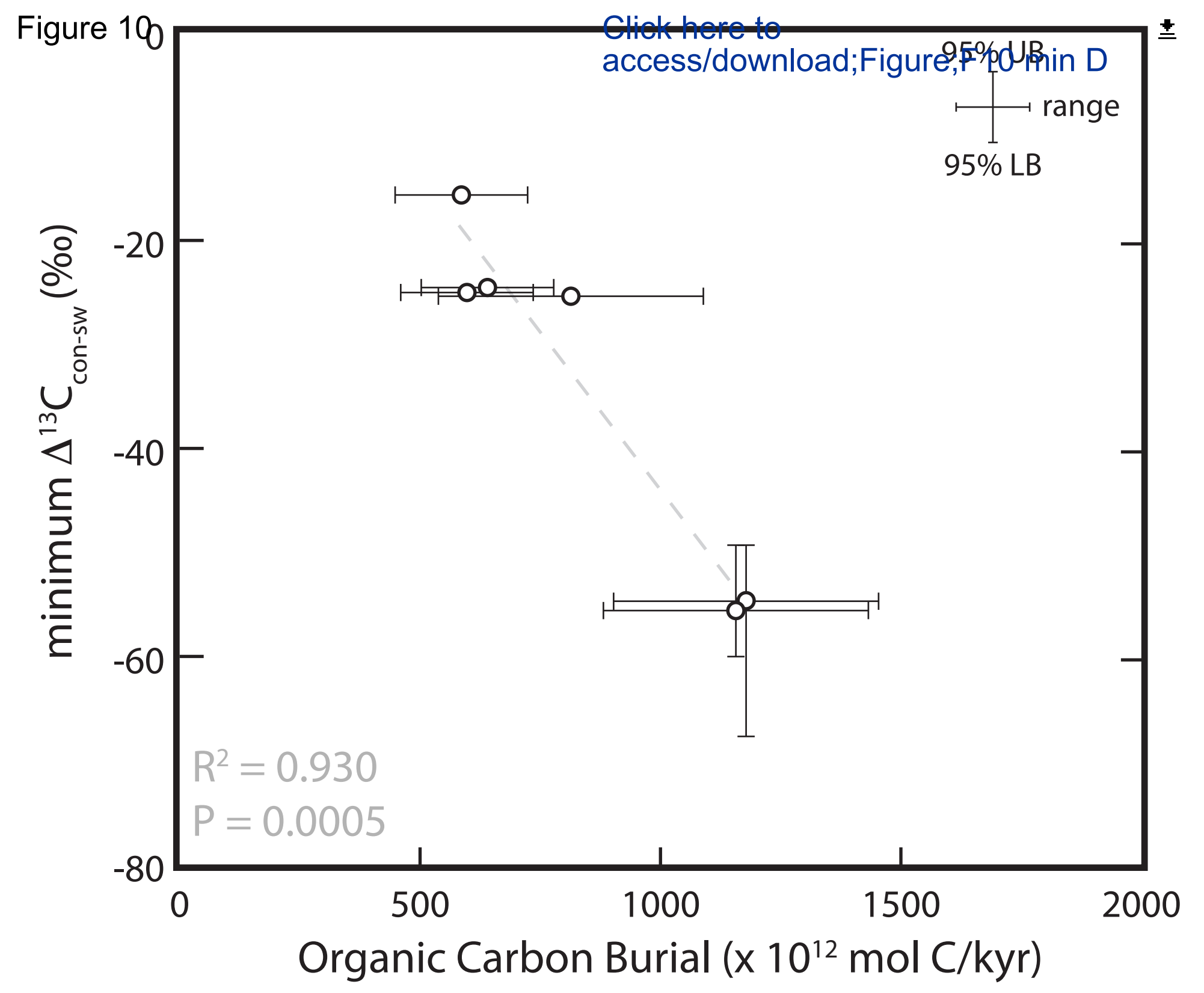

Figure 11

Click here to access/download;Figure;F11 TOC